UNIVERSITY OF GOTHENBURG

SAHLGRENSKA ACADEMY

Compartment model for radon-induced absorbed dose in lungs

Master's thesis

Sofia Hosseini

Essay/Thesis:	30 hp
Program and/or course:	Medical Physics
Level:	Second Cycle
Term/year:	Fall 2023
Supervisor:	Mats Isaksson and Christopher Rääf
Examiner:	Magnus Båth

Abstract

Essay/Thesis:	30 hp
Program and/or course:	Medical Physics
Level:	Second Cycle
Term/year:	Fall 2023
Supervisor:	Mats Isaksson and Christopher Rääf
Examiner:	Magnus Båth
Keywords:	Radon exposure, Human Respiratory Tract Model, time-integrated activity, cumulative activity, Absorbed dose, Lung dose

Inhalation of radon gas and radon daughters has since a long time been reported as the second leading cause of lung cancer after smoking. The biological hazards make it therefore important to quantify the absorbed doses from radon and radon daughters. The first aim of the study was to reconstruct the Human Respiratory Tract Model, presented by ICRP, to describe the biokinetics, i.e. movement of radon and radon daughters after inhalation for members of the public. The biokinetic model was implemented in the software tool Ecolego and was supplemented with Human Alimentary Tract Model and systemic models of radon, polonium, lead, and bismuth for a complete description of internal exposure. The final biokinetic model enables the user to acquire time-integrated activity (Ã) for combinations of 1) radon and radon daughters, 2) different modes of particle size distribution of radon daughters in air, 3) for members of the public of ages 3 months old, 1 year old, 5 years old, 10 years old, 15 years old and adults defined by ICRP and 4) genders for 15 years old and adults. The model was in a first step bench-marked against the internal dose calculation software Taurus, through comparison of Ã in the lungs, which resulted in approximately 20% relative bias between the implemented biokinetic model and Taurus. For an overall evaluation of the biokinetic model, the effective dose for radon daughters was calculated to be 18.22 mSv per WLM, which is in the range of values (7–21.1 mSv per WLM) obtained by other researchers. A secondary aim was to study how absorbed doses from emitted α-and β-particles following the decay of radon and radon daughters are distributed between tissues of the lungs. Absorbed doses were generated using the software program IDAC-Dose 2.1. In addition, values of S coefficients for combinations of source regions and target tissues inside the respiratory tract were incorporated in the software giving approximative values on absorbed doses and associated uncertainties. The absorbed dose from inhaled radon gas were found to be two orders of magnitude smaller than absorbed doses from inhaled radon daughters. The highest absorbed doses were, as expected, found to be from emitted α-particles from ^{218}Po- and ^{214}Po-decay in nearly all tissues of the lungs.

Sammanfattning

Inandning av gasen radon och radondöttrar är sedan länge ansett som den näst vanligaste orsaken till lungcancer efter rökning. Biologiska skador som uppstår i samband med intag av radon och radondöttrar gör det därför viktigt att kunna kvantifiera kroppens exponering. Syftet med projektet var att rekonstruera lungmodellen som är presenterad av ICRP, för att beskriva biokinetik, det vill säga fördelning av radon och radondöttrar mellan lungvävnaderna för allmänheten. Lungmodellen implementerades i programvaran Ecolego, och kompletterades med modell för matsmältningskanalen och systemiska modeller för radon, polonium, bly och vismut för att få en fullständig beskrivning av den interna exponeringen. Den framtagna biokinetiska modellen gör det möjligt att erhålla tidsintegrerad aktivitet (Ã) för olika kombinationer av 1) radon och radondöttrar, 2) fristående radondöttrar, eller olika tillstånd av bundna radondöttrar 3) för av ICRP-definierade åldrarna 3 månader, 1 år, 5 år, 10 år, 15 år och vuxna, och 4) för olika kön för 15 år gamla och vuxna. Modellen utvärderades i ett första steg mot Taurus som är en programvara för interndosimetri, via jämförelse av Ã i lungor, som resulterade i ett relativt fel på ungefär 20% mellan implementerad biokinetisk modell och Taurus. För en helhetsbedömning av den biokinetiska modellen, beräknades effektiv dos från radondöttrar som gav ett värde på 18,22 mSv per WLM, som ligger inom intervall (7–21,1 mSv per WLM) angiven av andra forskare. Studiens andra syfte var att ta fram hur absorberad dos från α- och β-partiklar som emitteras i samband med radioaktiva sönderfall av radon och radondöttrar fördelas mellan lungvävnaderna. Värden på absorberade doser beräknades i programvaran IDAC-Dose 2.1. Dessutom inkorporerades det i programmet värden för S koefficienter för källorgan och målvävnader i lungor, vilket gör det möjligt att få ungefärliga värden på absorberad dos och tillhörande osäkerheter. Absorberad dos från inhalerad radon beräknades vara hundra gånger mindre än absorberad dos från inhalerade radondöttrar. Den högsta dosen i nästan alla lungvävnader kom som förväntat från α-partiklar som emitteras från sönderfall av ^{218}Po och ^{214}Po.

Table of contents

1. Introduction 1
1.2. Aim 1
1.3. Background 1
1.4. Theoretical framework 3
1.4.1. Internal dosimetry 3
1.4.2. Biokinetic models 5
1.5. Dosimetry for lung doses 11
2. Material and method 13
2.1. Construction of compartment model 13
2.1.2. Digression: treatment of inhaled radon progeny and radon progeny produced after inhalation 14
2.2. Deposition of particles in the human respiratory tract regions 15
2.3. Simulation 17
2.4. Dosimetry of radon and radon progeny 17
2.4.1. Calculating effective dose 19
2.4.2. Study of doses to respiratory tract regions for an arbitrary condition 20
2.5. Integration of biokinetics and dosimetry in Ecolego for direct access of absorbed doses for an initial set of deposition conditions 21
3. Results 22
4. Discussion 26
4.1. Biokinetic model 26
4.2 Dosimetry 27
4.3. Improvements 31
5. Conclusion 31
Acknowledgements 32
Appendix A: Parameter values for transfer coefficients in HRTM and HATM 33
Appendix B: Systemic models 33
B-1: Radon 33
B-2: Polonium 35
B-3: Bismuth 37
B-4: Lead 38
B-5: Treatment of radionuclide as progeny of lead 40
B-6: Treatment of radionuclide as progeny of radon 41
Appendix C: Polynomials describing fractional deposition in the lung regions 43

References 49

1. Introduction

Radon was formally associated with an increased risk of lung cancer in 1986 by World Health Organization (WHO, 1986). The information was built on cohort studies on underground uranium miners, which in a thorough analysis of epidemiological studies published by the International Commission on Radiological Protection (ICRP) was further solidified (ICRP, 1993b). Since then, comprehensive epidemiological studies have been done and concluded exposure to radon and radon progeny as the second-important cause to lung cancer after smoking (ICRP, 2014; WHO, 2009). Based on a meta-study (Darby et al., 2005) including 13 European case-control studies, there is an excessive relative risk of 16% for lung cancer per 100 Bq/m^3. Based on the collective results of the case-control studies, the investigators concluded residential radon to be the cause of 2% of all deaths in cancer in Europe. The relative risk of lung cancer because of exposure to radon was estimated to be equal for smokers and non-smokers (Darby et al., 2005). According to United Nations Scientific Committee on the Effects of Atomic Radiation (UNSCEAR), radon and its progeny constitute 48% of the global annual effective dose of natural background radiation, which is 2.4 mSv (UNSCEAR, 2000).

Because of the aforementioned reasons, it is important to quantify the hazard of radon from the point of view of radiation protection. ICRP Task groups investigate biokinetics of different elements in the human body to produce biokinetic models and derive dose coefficients for specific aerosol characteristics and equilibrium factors for members of the public of different age. However, information on the amount of absorbed dose for arbitrary conditions are not complete.

1.2. Aim

The aim of this study was to use the ICRP human respiratory tract model (HRTM) (1994, 2015), the ICRP alimentary tract model (HATM) (2006) and relevant systemic models to describe the biokinetics of radon and radon daughters (progeny) inside the body for members of the public under various environmental conditions listed below:

- different age groups,
- unattached and attached radon progeny,
- and for various concentrations of radon and radon progeny.

A secondary aim was to study how absorbed dose from emitted α- and β-particles following the decay of radon and radon progeny are distributed between respiratory tract regions.

1.3. Background

The ICRP Publication 126 (2014) provides insights into radon exposure relevant to radiological protection. Based on researches, conducted across various countries, the report describes the characteristics of radon source and radon exposure as the following. Radon (Rn) is a gaseous decay product of naturally occurring radionuclides uranium-238, uranium-234 and thorium-232, which are present in Earth's crust in varying concentrations. As radon

is a gas, it can diffuse through pores and fractures in the soil and is therefore present in the air. The shorter-lived radon isotope, radon-219 (^{219}Rn, $t_{1/2}$ = 4 seconds) decays before it travels far from its decay location and is therefore not related with biological hazards. The principal biological hazard associated with lung cancer is due to radon-222 (^{222}Rn, $t_{1/2}$ = 3,82 days) and its decay products. Exposure to radon-220 (^{220}Rn) usually does not present a problem in radiation protection, except for indoor air from building materials in some traditional housing. Due to its short half-life of 56 seconds, ^{220}Rn does not compose substantial indoor air activity concentration (ICRP, 2014). Although there is interest in research about dose distribution from ^{220}Rn and its progeny, it is beyond the scope of this study and will therefore not be treated.

Typical values of radon concentration in outdoor air have been approximated to 10 Bq/m^3 (UNSCEAR, 2009). The largest fraction of exposure to ^{222}Rn happens indoors, which according to UNSCEAR is estimated at approximately 40 Bq/m^3 for world average concentration. Indoor air concentrations as high as 84 000 Bq/m^3 have also been measured (UNSCEAR, 2009). The reference value established by the Swedish Radiation Safety Authority (SSM) is 200 Bq/m^3 for homes and workplaces (SSM, 2023). Main contributing factors affecting radon concentration in buildings are pressure differences between indoors and outdoors due to ventilation rates and meteorological conditions, beside building material and cracks in them (ICRP, 2014).

The decay products of ^{222}Rn are isotopes of polonium (Po), lead (Pb) and bismuth (Bi) which can be divided into two groups, the short-lived and the long-lived radon progeny. The short-lived progeny consists of ^{218}Po ($t_{1/2}$ = 3.1 min), ^{214}Pb ($t_{1/2}$ = 26.8 min), ^{214}Bi ($t_{1/2}$ = 19.9 min) and ^{214}Po ($t_{1/2}$ = 164.3 µs). The long-lived progeny are ^{210}Pb ($t_{1/2}$ = 22.2 a), ^{210}Bi ($t_{1/2}$ = 5.013 d) and ^{210}Po ($t_{1/2}$ = 138.377 d) (Brudecki et al., 2014; ICRP, 2015). Diagram over production and decay scheme of ^{222}Rn can be viewed in Figure 1.

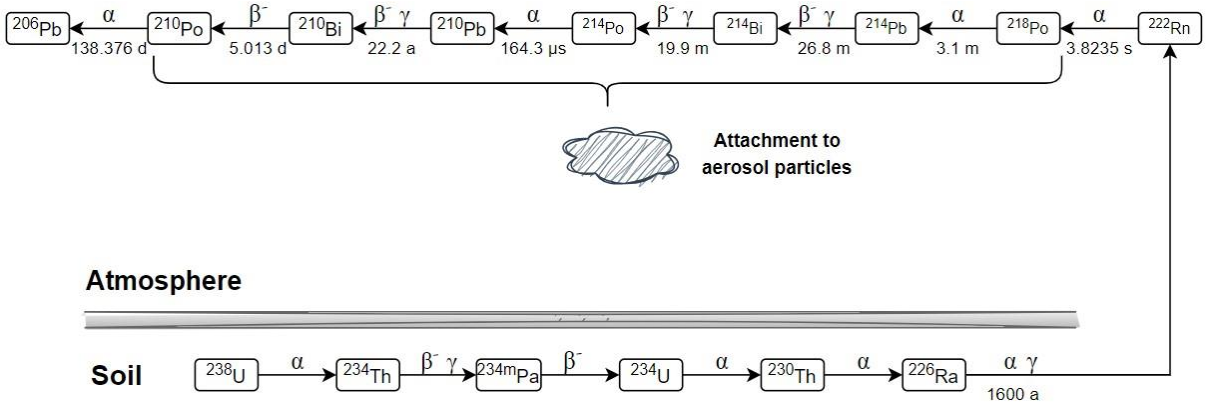

Figure 1. Production and decay scheme of ^{222}Rn. Redrawn from (Brudecki et al., 2014).

According to previous studies, the highest organ dose from radon inhalation is to the source organ, the lungs in this case (Kendall & Smith, 2002; Sharma et al., 2018). It is now understood that the dominant contribution to dose is from the inhaled short-lived radon progeny, mainly the α-emitting radon progeny. Since radon is a noble gas, nearly all the inhaled gas will be exhaled. The short-lived radon progeny are however solid elements,

which attract trace gases and water molecules quickly in less than one second after production. These progeny are referred to as unattached radon progeny (Kendall & Smith, 2005). The unattached radon progeny can then bind to ambient aerosols forming so called attached radon progeny (ICRP, 2017).

The size distribution of the radon progeny is a dominant parameter related to the amount of radon progeny inhaled and the site of deposition after inhalation (Porstendörfer, 1994, 2001). The size distribution of unattached progeny (also called cluster mode) is suggested to follow a unimodal log-normal distribution with particle sizes varying between 1.5 and 1.7 nm. The appropriate size for dose calculation purposes suggested by ICRP is 1 nm with geometrical standard deviation, σ_g, of 1.3 (ICRP, 2017). For attached radioactive progeny the aerosol size is affected by the aerosol conditions of the room. For instance, activities like cooking and smoking attribute to different particle sizes (Porstendörfer, 1994). Studies show that the attached radon progeny have a trimodal activity size distribution which consists of three log-normal modes, namely nucleation mode, accumulation mode and coarse mode that are defined as aerosol sizes in ranges 10–100 nm, 100–450 nm and greater than 1µm respectively, characterized by activity median aerodynamic diameter (AMAD) and activity median thermodynamic diameter (AMTD, < 300 nm) (ICRP, 2017; Porstendörfer, 2001). The differences in activity size distribution between the radon progeny are shown to be negligible. Therefore, the same activity size distribution is assumed for all the elements for calculation purposes (ICRP, 2017).

The air activity concentration associated with radon progeny is constituted of 10% unattached and 90% attached radon progeny in average for domestic environments (Kendall & Smith, 2005; Porstendörfer, 1994). When inhaled, the radon progeny will diffuse and distribute heterogeneously on the surface of the respiratory airways of the lung (Kendall & Smith, 2005). Because of their short half-lives, some of the radon progeny will decay and deposit energy to the lung tissue before clearance takes place, leading to absorption into blood or further distribution to the alimentary tract (Harrison, 2009). For a complete view of the internal exposure from inhalation, it is therefore necessary to include also the biokinetic model for alimentary tract and systemic circulation.

1.4. Theoretical framework

1.4.1. Internal dosimetry

The purpose of internal dosimetry is to determine the spatial and temporal energy deposition following heterogenous particle-specific distribution in organs and tissues of the body, associated with radionuclide intake (Andersson et al., 2022). Doses to organs and tissues cannot be measured, therefore the doses need to be calculated instead. The absorbed dose D, to target tissue r_T, at a time t, from radionuclide intake at time t_0, is expressed as:

$$D(r_T,\tau) = \sum_{r_S} \tilde{A}(r_S,\tau) \cdot \frac{\sum_{i,R} E_{i,R}\, Y_{i,R}\, \emptyset_{i,R}(r_T \leftarrow r_S, E_{i,R}, t)}{M(r_T,t)} = \sum_{r_S} \tilde{A}(r_S,\tau) \cdot S(r_T \leftarrow r_S),$$

where τ is the time between t_0 and t. Ã is the time-integrated activity, also known as cumulative activity in the source region r_s, during the integration period τ, with τ being up to 50 and 70 years for adults and children respectively. The indices R and i refer to the type of radiation and energy of radiation type R respectively. E is the emission energy during decay, and Y is the yield of energy i for radiation type R (ICRP, 1994, 2016). The product of $E_{i,R}$ and $Y_{i,R}$ is known as equilibrium absorbed dose quantity Δ (ICRP, 2008). ϕ is absorbed fraction (AF), defined as the fraction of the emitted energy per radionuclide transformation in a given source region that is deposited in a given target tissue at time t, and M is the mass of the target tissue (ICRP, 1994, 2016). The quotient of ϕ and M is called specific absorbed fraction (SAF). For β-emission, the summation is replaced by an integral over the energy interval of the β-particle spectrum (ICRP, 2016). The equation for absorbed dose can be simplified as the product of Ã and the absorbed dose rate coefficient (S coefficient), formerly known as specific effective energy (SEE). The S-coefficient is defined as dose rate in target region per nuclear transformation in source region and is expressed in Gy $(Bq\ s)^{-1}$ (ICRP, 1994).

The cumulative activities in source regions are obtained with the use of biokinetic models. Biokinetic models are mathematical representations that describe time-dependent movement of radionuclides in the body, through usage of organs and tissues that are important for accumulation of radionuclides. In the models, the characteristics of uptake, retention in different regions and excretion through different pathways are considered. The interactive property of the regions, represented by transfer rates, makes these models into so-called compartment models, which are described by systems of first-order differential equations (Andersson et al., 2022; Isaksson, 2003). For such systems, the transfer coefficient is independent of time and concentration in the individual compartments, i.e. organs and tissues. The flow to another compartment is given as the product of activity in the initial compartment and transfer coefficient. The activity for each time step since intake, can be calculated by numerically solving the differential equation for each compartment. By integrating the activity over a given period of time can Ã in this way be obtained (Brudecki et al., 2014; Isaksson, 2003).

The biokinetic models describing the respiratory and alimentary tract are used to define the movement of radionuclides within these systems, while circulation in blood is described by systemic models, which range in complexity depending on the element studied (ICRP, 2015).

Dosimetric models describe the geometrical relationship of anatomical structures and are used to calculate the deposited energy in the target tissue from each disintegration in the source region taking into account the energy and yield of the emission (Harrison, 2009). The reference biokinetic and dosimetric models are published by the internationally recognized organization ICRP. ICRP utilizes the models mostly to compute dose coefficients which are necessary in assessment of reference levels for existing exposure situations for workers and members of the public (Harrison, 2009).

1.4.2. Biokinetic models

1.4.2.1. Human Respiratory Tract Model

The Human Respiratory Tract Model (HRTM) is divided into two tissue types which are further categorized into regions based on radiation sensitivity. The first tissue, the extrathoracic airways (ET), constitutes of the regions anterior nasal passage (ET_1); and the posterior nasal passage, pharynx and larynx (ET_2). The second tissue, the thoracic (TH) airways, includes the bronchial (BB) region, the bronchiolar (bb) and the Alveolar-Interstitial (AI, also shortened as ALV) region. All regions, except ET_1, are connected to lymph nodes. The morphological depiction is shown in Figure 2.

The air conducting airways of the thoracic system are bifurcated into narrower airways, known as generations. The regions BB, bb and ALV have corresponding generations 0–8, 9–15 and 16–26 respectively, with each generation having a characterized length and diameter.

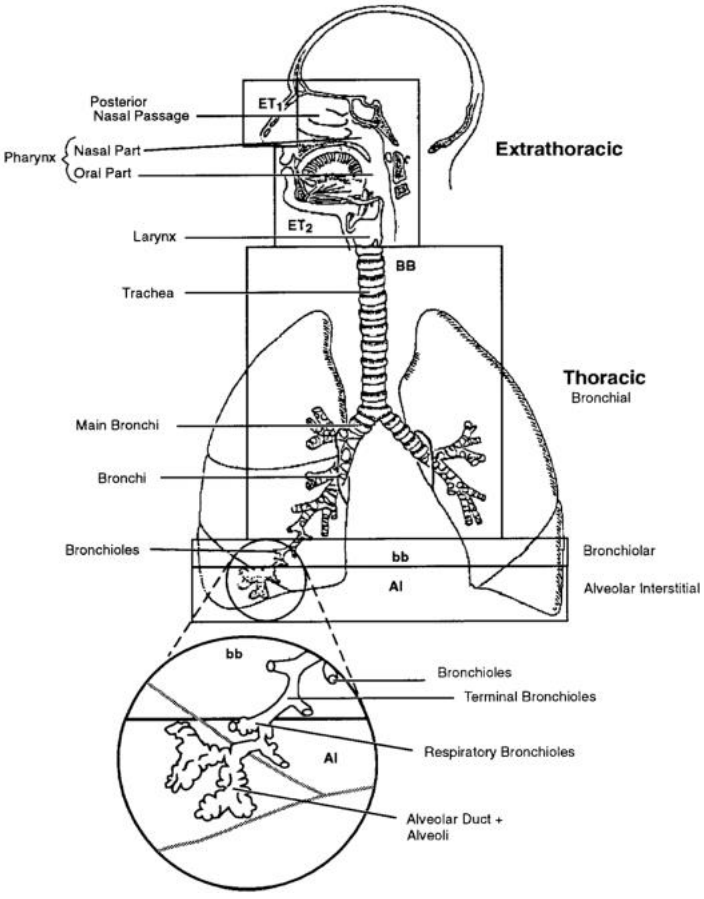

Figure 2. Morphological description of the respiratory tract. Taken from figure 3.1 in ICRP 130 (2015). Used with permission from ICRP.

Deposition fraction refers to the fraction of the molecules entering the body through inhalation and remaining after exhalation. The regional deposition fractions of unattached and attached radon progeny are primarily determined by the particle size. Other determining factors are the tissue's efficiency in removing airborne particles and breathing

pattern, where the latter is dependent of age and exercise level (ICRP, 1994; Zhu et al., 2018). The regional depositional fractions tabulated in ICRP Publication 66 are given for aerosols with log-normal particle size distribution (ICRP, 1994, 2015; Porstendörfer, 1994). For gases, deposition is dependent upon the chemical form of the gas, where the radionuclide's solubility and reactivity will determine uptake from the respiratory tract walls. The default regional deposition for gases are 20% ET_2, 10% BB, 20% bb and 50% AI (ICRP, 2015).

The HRTM applied in this study follows the revised model described in ICRP publication 130 (2015), which contains major changes in relate to clearance compared to the original model described in ICRP publication 66 (1994). In HRTM, clearance is defined as the particle transport and absorption into blood. The paths of clearance from the respiratory tract, including ET_1, are through nose blowing, absorption into blood and particle transport to alimentary tract, lymphatics and lymph nodes. The clearance rates (shown in Figure 3) are assumed to be independent of age, sex, material and element. The particles retained in ET_1 are transported by one third through nasal blowing and two thirds are cleared further to ET_2', with transfer coefficients 0.6 and 1.5 respectively. In contrast to the original HRTM, the oral passage is no longer included in ET_2, therefore, the compartment was redefined as ET_2'. In addition, the clearance from BB and bb towards the throat is described by one phase, instead of two, hence redefined as BB' and bb' respectively (ICRP, 2015).

A fraction of 0.2% of the initial deposit in regions ET_2', BB' and bb' is long-term retained (sequestered) in the airway walls and are subsequently denoted as ET_{seq}, BB_{seq} and bb_{seq} respectively. The particles are then transported to lymphatics and lymph nodes (LN). The clearance towards the trachea (i.e., ALV $\rightarrow$ ET_2') happens faster, and is therefore denoted with increasingly higher transfer coefficients. The particles in ALV are slowly cleared to the interstitium (INT) for very long-term retention, from where it clears very slowly to the thoracic lymph nodes (LN_{TH}) (ICRP, 2015).

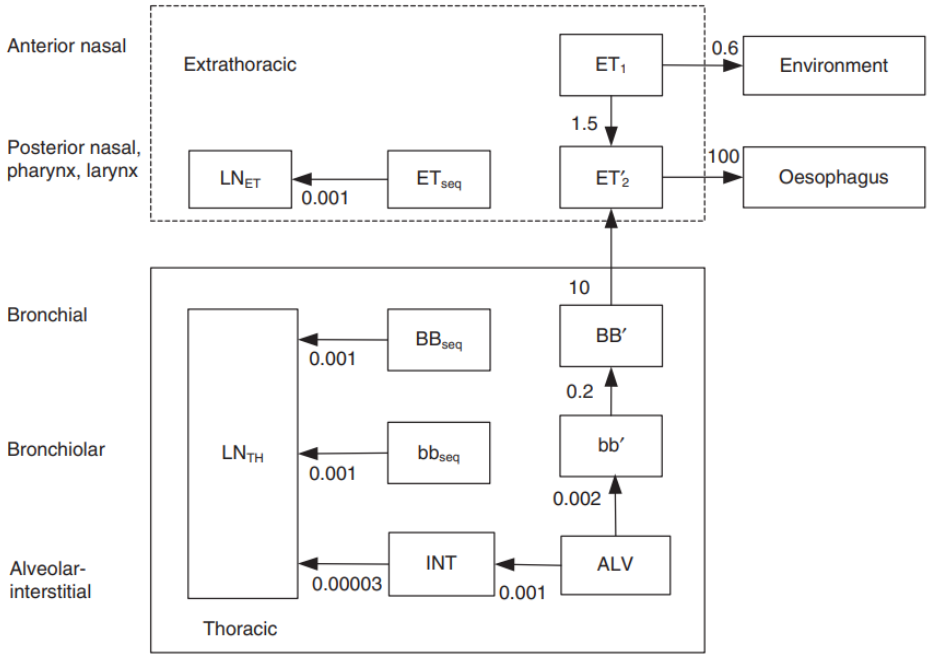

Figure 3. The diagram shows the revised time-dependent particle transport in the respiratory tract with the corresponding transfer coefficients expressed in d^{-1}. A fraction 0f 0.2% of the initial deposit in the regions ET_2', BB' and bb' are long-term retained in the regions ET_{seq}, BB_{seq} and bb_{seq} respectively. The compartments of BB', BB_{sec}, bb', bb_{seq}, ALV and INT together make up the lungs of the human body. Taken from figure 3.4 of ICRP Publication 130 (2015). *Used with permission from ICRP.*

The process of absorption is divided into two stages, dissolution and uptake, with both processes having time-dependent clearance rate, determined by whether the material clears at fast, moderate or slow (F, M, S) rate. Dissolution is defined as the breakdown of the particles into absorbable materials. Uptake is the process of absorption of the absorbable and dissolved materials into blood. The absorption rate into blood is assumed to be the same for all compartments of the respiratory tract except ET_1, from where no absorption occurs. For gases, assuming instantaneous uptake into blood is recommended (ICRP, 2015).

The dissolved materials are still available for transport between compartments in the respiratory tract. To consider this, the ICRP has suggested the time-dependent compartment model for absorption in Figure 4 to describe dissolution and uptake. This absorption model is an alternative to a standard model. The alternative method is used to account for rapid dissolution rate. The differences in resulting values are, according to ICRP, small, why ICRP recommends using the standard model to avoid unnecessary complex models to deal with. An element with absorption model according to the standard model can also be described with the alternative model. However, the reverse is not true.

In the alternative model, the “particles in the initial state” represent the respiratory tract compartments in which deposition occurs. From each compartment, the particles are then transferred to the associated compartment in “particles in transformed state” to take account of the particle transport of the dissolved material. Some elements have an intrinsic property to attach to the respiratory tract compartments and therefore clear slower, symbolized with “bound material”. The values for the transfer coefficients [d^{-1}], are the

dissolution rate, s_p, transformation rate, s_{pt}, and the final dissolution rate, s_t, and are calculated as:

$$s_p = s_s + f_r(s_r - s_s)$$
$$s_{pt} = (1 - f_r)(s_r - s_s)$$
$$s_t = s_s.$$

From the equation, f_r and $(1\text{-}f_r)$ stand for the rapid dissolution fraction and slow dissolution fraction, respectively, with associated dissolution rate s_r, and s_s respectively. The absorption parameter values for radon progeny are collated in Table 1.

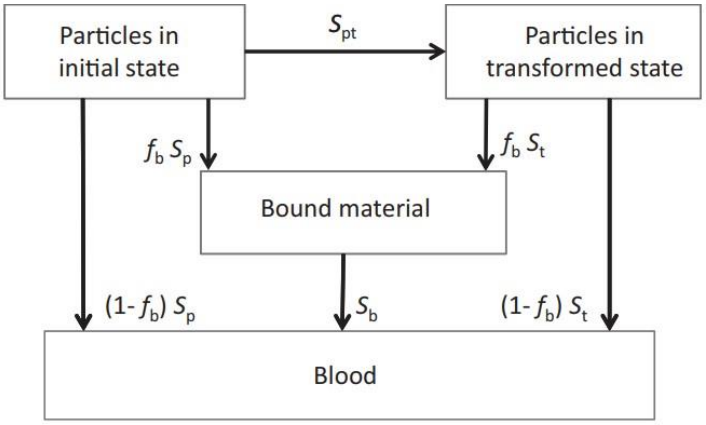

Figure 4. Compartment model for time-dependent absorption into blood. Taken from figure 3.5. (b) of ICRP Publication 130. Used with permission from ICRP.

Table 1. Absorption parameter values for inhaled radon progeny polonium, bismuth and lead. f_r and $(1\text{-}f_r)$ stand for the rapid dissolution fraction and slow dissolution fraction respectively with corresponding dissolution rate s_r, and s_s. The bound fraction of elements is described with f_b, and the uptake transfer rate s_b. The absorption fractional from alimentary tract is represented with f_A. ICRP has used this set of parameter values for calculation of dose coefficients for radon progeny aerosols given in Table 12.6 of ICRP Publication 137. The parameter values are taken from Table A.2 of ICRP Publication 137. (ICRP, 2017).

Inhaled radon progeny	**Dissolution parameter values**			**Uptake parameter values**		**Absorption from the alimentary tract, f_A**
	f_r	s_r [d^{-1}]	s_s [d^{-1}]	f_b	s_b [d^{-1}]	
Polonium	1	3	-	0	-	0.1
Lead	0.1	100	1.7	0.5	1.7	0.20
Bismuth	1	1	-	0	-	0.05

1.4.2.2. Human Alimentary Tract Model

Figure 5 illustrates the structure of the Human Alimentary Tract Model (HATM). The relation of HRTM and systemic model with respect to HATM is also depicted. The inhaled activity can transport to the oesophagus by mucociliary action. The material in the oesophagus is fractionated into two compartments, expressing fast and slow removal. The sequential transfer of material is continued through stomach, small intestine, right colon, left colon,

rectosigmoid colon and faeces. The values of transfer coefficients are dependent of age, sex and are based on total diet for the different transfer steps, when no relevant information is available of the material. The parameter values for transfer coefficients are tabulated in Appendix A: Parameter values for transfer coefficients in HRTM and HATM.

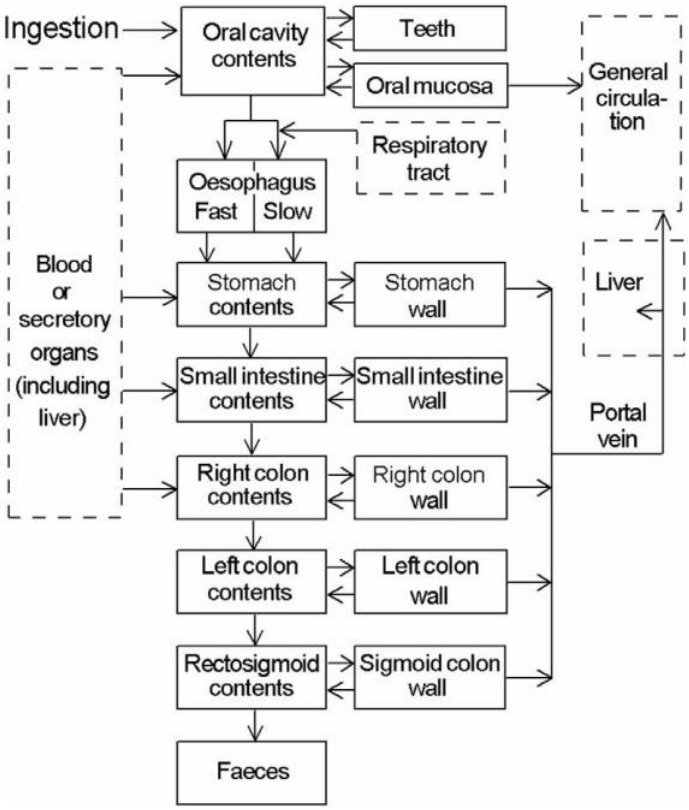

Figure 5. Structure of HATM. The respiratory tract and blood are shown as dashed boxes. Taken from figure 5.1 of ICRP Publication 100 (2006). Used with permission from ICRP.

Absorption does predominantly take place from the small intestine. Absorption from the segments is thought to occur from the segment wall to portal vein, which passes through the liver and continues to the general circulation. In HATM, the fraction activity absorbed is denoted f_A, which is defined as the fraction of the total activity entering the alimentary tract that is absorbed, from all compartments of the HATM. In most cases, only the total absorbed fraction is specified for different elements and its radioisotopes, therefore the standard assumption is that all absorption occurs from the small intestine, so that $f_A = f_{IS}$, where f_{IS} is the absorbed fraction from the small intestine. By default, there is also no recycling, meaning no recirculation of materials between the segment walls and segment contents in the alimentary tract (ICRP, 2006, 2015). Secretion of activity from blood back to contents of alimentary tract are assumed to be reabsorbed (ICRP, 2015).

The element and its chemical form are primary factors determining the extent of intestinal absorption. For radioactive isotopes that are transferred from the respiratory tract to the alimentary tract, the fractional absorption from the alimentary tract, f_{al}, is derived as the product of f_r and f_A. Where f_r is the fraction of the soluble element that is available for

absorption from alimentary tract and f_A is the fraction of the soluble material that is absorbed to blood from alimentary tract (ICRP, 2015).

1.4.2.3. Systemic biokinetic models

The systemic biokinetic models are developed by ICRP to explain the movement of individual elements in the blood circulation, with the guiding principle that radioisotopes of an element behave in the same way as the stable isotopes of the element.

For some elements, one organ is represented by multiple compartments to illustrate the different fates of the element in the organ. For instance, kidney consists of two compartments in the model for polonium to describe the different outcomes after element-uptake, where the polonium in kidney 1 is transferred to urinary bladder, while polonium in kidney 2 is returned to blood (ICRP, 2017).

For the structure of the systemic model for radon and the isotopes of radon progenies, the reader is directed to Figure 8 to Figure 11 in Appendix B: Systemic models. The applied systemic models for the radon progeny are those described in ICRP publication 137 (2017), while the adopted systemic model for radon is based on the newly developed model by Samuels et al. (2023) with age- and sex-specific transfer coefficients.

The removal from urinary bladder content is assumed to be 40 d^{-1}, 32 d^{-1} and 12 d^{-1} for age groups 3 months-old, 1 year-old and above 1 year-old, respectively, for all elements, according to table 3 of ICRP Publication 71 (ICRP, 1995). As a side note, the age range for each specific age group is defined as (ICRP, 1995):

- 3 months: from 0 to 12 months old,
- 1 y: from 1 y to 2 y,
- 5y: from 2 y to 7 y,
- 10 y: from 7 y to 12 y,
- 15 y: from 12 y to 17 y,
- Adult: more than 17 y.

The progeny produced in the systemic circulation are categorized into either i) progeny produced as decay product of radon or ii) progeny produced as decay product of lead. The systemic biokinetic model for the first type mentioned is based on modifications on the second type. The changes include four supplementary compartments: fat 1, fat 2, adipose breast tissue and glandular breast tissue. All the four compartments are explicit to the systemic model of radon. These modifications allow the elements of the chain members to be removed from its point of origin.

The changes that need to be introduced to account for a progeny as a decay product of a member of the radon decay chain are the same as if the radionuclide was a decay product of lead. Similar guideline as in i) is implemented, where designated source regions explicit to the parent are added to the characteristic systemic model of the daughter.

'Independent kinetics' is assumed for progeny produced in radioactive decay of the parent inside the body, which means individual tracking of the chain members of the parent (ICRP, 2017). More about treatment of radionuclides as progeny of lead and radon can be found in

section B-5: Treatment of radionuclide as progeny of lead and B-6: Treatment of radionuclide as progeny of radon. These sections are preceded by sections on systemic models of radon and radon progeny for a deeper understanding.

The compartment 'other' in the systemic models comprises source regions r_s, not explicitly defined in the characteristic model of the element. The compartments of HRTM and HATM are consequently not included in this 'other'-compartment. The SAF from 'other' to target region is calculated as:

$$SAF(r_T \leftarrow r_{other}) = \frac{1}{M_{other}} \sum_{r_s} M_{r_s}\ SAF(r_T \leftarrow r_s),$$

where the summation is over the masses of the source regions M_{r_S}, contained in 'other', and M_{other} is the total mass of the components of 'other' (ICRP, 2016).

1.5. Dosimetry for lung doses

The purpose of respiratory tract dosimetry is to evaluate the doses to the radiosensitive target regions of the respiratory regions, defined as the progenitor cells for respiratory tract cancer from radionuclides retained in source regions (ICRP, 1994). Fundamental for dosimetric calculations are 1) time-integrated activity in source regions, 2) decay scheme data and 3) specific absorbed fraction. ICRP Publication 107 and Publication 133 present nuclear decay data and specific absorbed fraction for reference adult, respectively (ICRP, 2008, 2016).

The original SAFs are given in ICRP Publication 66 and are derived with respect to anthropomorphic phantoms. The improved adopted SAFs are produced with respect to reference computational phantoms that are based on medical imaging data, obtained with computed tomography and magnetic resonance imaging. The SAFs are compiled for monoenergetic electrons, photons and alpha particles. The radiation transport for combinations of source and target regions have been simulated with Monte Carlo technique for the computational phantom representing the geometry of the reference individuals (ICRP, 2016).

For the calculation of lung doses, the lungs are represented by the regions BB, bb and AI (ICRP, 1994). The regions of extrathoracic and thoracic tissues are characterised into further regions to take account of source regions and target regions. The simplified geometrical model shown in Figure 6, has been utilized to represent the orientation of the homogeneously distributed radionuclides in source region and target cells in target region. In each case, the model is constituted of a cylinder with appropriate average inner calibre based on the generations of the respiratory tract region, where the layer of tissue containing the target cells is assumed to lie at certain depth below the epithelial surface. The depth of radionuclide sources and target cells for ET_2, BB and bb are shown in Figure 6.

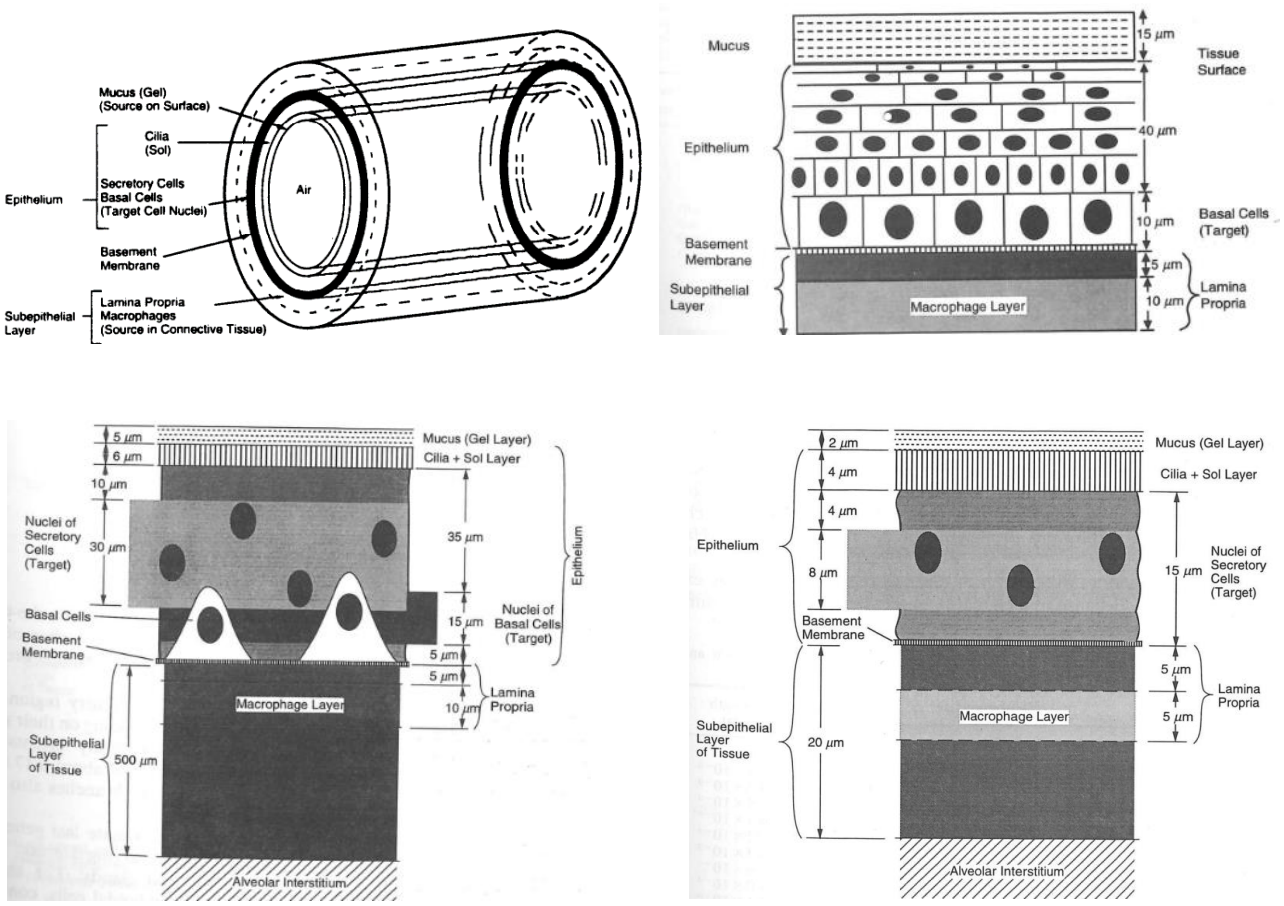

Figure 6. Top left: a simplified geometric cylinder model adapted by ICRP Publication 66 for depiction of source and target regions in respiratory tract regions, of ET_2 in top right, BB in bottom left and bb in bottom right. Taken from (ICRP, 1994). Used with permission from ICRP.

The target tissue for ET_1 is the basal cells. The wall of nasal vestibule contains keratinised squamous epithelium (skin). Skin is considered to be impervious to radionuclide sequestration and absorption, therefore limiting the location of radionuclide source to only skin surface.

The target cells for ET_2 are also basal cells. Three distinct distribution of radionuclide source are defined for ET_2. 1) The mucus layer which is represented in the compartment model by fast particle transport. 2) The macrophage layer represented by sequestered compartment and, 3) the 5 µm layer below basement layer represented by 'bound material'.

The target cells for BB are secretory and basal cells. The radionuclide sources of BB are categorized into five distinct distributions. 1) the mucus layer and 2) sol layer, which in HRTM applied in ICRP Publication 66 is represented by fast and slow surface transport compartments, respectively; in the revised HRTM of ICRP Publication 130, fast and slow surface transport are summed into BB' compartment. 3) macrophage layer, which is represented by the compartment 'BB_{seq}', 4) material chemically bound in the 5 µm layer below basement membrane, represented by compartment 'bound material' and 5) the energetic alpha and beta emitters located in AI.

The target cells for bb are secretory cells, and the radionuclide sources are categorized in the same manner as that for BB. For AI, the target cells are homogeneously distributed throughout the whole tissue so that the whole tissue is regarded as target region. Since energy is distributed among a greater target mass in AI, the cross dose is negligible compared to the self-dose of the source regions (ET, BB and bb) themselves, so that the cross absorbed fraction is assumed zero. While the self-absorbed fraction is assumed to be unity for non-penetrating radiation.

Depending on the geometry between source region and target region, some fraction of the decay energy will be deposited in the target region. For distinct source and target regions, this is called crossfire. Crossfire is thus defined as the deposition of energy from a distinct source region to a target region. Doses from crossfire are often needed for penetrating photon radiation. For non-penetrating α- and β-radiation, the source and target region are mostly the same. Damage caused by radon are principally caused by α- and β-particles that are emitted during the decay of short-lived radon progeny giving rise to high local absorbed doses (Harrison, 2009; Zhu et al., 2018). In fact, the dominating dose to the lungs following inhalation of radon progeny are from the α-emitting particles of ^{218}Po and ^{214}Po (ICRP, 2014)

2. Material and method

The biokinetic model was conducted in the modelling software tool Ecolego (Version 8.0, AFRY, Sweden). The idea behind the software is to define small building blocks of a system like, for example, biokinetic and ecological systems to be able to construct the whole dynamics. The building blocks can represent compartments, transfer coefficients, parameter values etc. Favourable features such as ordinary differential equation (ODE) toolbox and radionuclide toolbox make it possible to solve linear and non-linear ODE and automatically take account of decay and ingrowth of radionuclides over time in each compartment, respectively. Another benefit of the radionuclide toolbox is that it features a database containing the relationship between the decay products such as decay mode, decay energies and decay constant. Furthermore, Ecolego has the functionality of creating sub-systems to encompass related compartments into one module. The sub-systems can shrink or widen to easier manage the whole compartment model (Ecolego, 2023).

2.1. Construction of compartment model

Initially, radon and the short- and long-lived radon progeny were imported from the radionuclide database since some building blocks of the model are element-specific. The compartments for the human respiratory & alimentary tract and systemic model were integrated together, with the momentary activity in each compartment being dependent on the radionuclide, aerosol size, and age of the subject. For 15-year-olds and adults, also the subject's sex was introduced as a dependency factor.

The movement of material between compartments was represented by transfer blocks. The value of transfer coefficients used for transfer between compartments of HRTM and HATM are shown in Figure 3 and Table 15, respectively. The mucociliary action towards the

alimentary tract was in the transfer blocks indicated as 90 % of total outflow from ET_2' clearing to the fast oesophagus and the rest to the slow oesophagus.

ICRP (2015) presents two absorption structure models to consider dissolved material that is still available for clearance in the respiratory tract regions. One of the models (i.e. the alternative model) was mentioned in Figure 4 of section 1.4.2.2. Human Alimentary Tract Model , which is the one applied here. Previous studies on the topic of absorption model for radon and its decay products from respiratory tract to blood were found to be rare, why the alternative model was applied in this study to acquire higher accuracy. Moreover, 'independent biokinetic' was applied for radon decay products produced in the respiratory tract, implying that absorption parameter values are determined based on the current element, and not on those of the parent (ICRP, 2015).

The absorbable transfer coefficient, $\lambda_{SI,B}$, from small intestine is given by:

$$\lambda_{SI,B} = \frac{f_{al}\,\lambda_{SI,RC}}{1 - f_{al}}.$$

where $\lambda_{SI,\,B}$ is the transfer rate to blood, $\lambda_{SI,\,RC}$ is the transfer rate from small intestine to right colon and f_{al} is absorption fraction from alimentary tract (ICRP, 2015). For radon, absorption occurs from small intestine to liver. The value of $\lambda_{SI,RC}$ was extracted from tabulated data on age- and sex- specific transfer coefficients derived by Samuels et al. (2023).

To be able to handle the systemic models easier, the biokinetic systemic tissues that are shared between two or more elements or are unique to one element were identified based on physiological properties of the compartment. Element-specific transfer coefficients were used to take account of the element-dependent structure of systemic models. For example, the compartment 'urinary bladder contents' is mutual for all radon progeny elements. Therefore, only one such compartment was defined in the software. The value of the transfer coefficient to urinary bladder contents was then assigned to differ for each element. In addition to element, the transfer blocks were also assigned to be dependent on age and sex for systemic compartments of radon and dependent on age for systemic compartments of lead. The transfer coefficients for systemic models can be viewed under associated element in Appendix B: Systemic models.

2.1.2. Digression: treatment of inhaled radon progeny and radon progeny produced after inhalation

A question that arose for us in the process was about how the compartment model would be able to distinguish between inhaled radon progeny following the characteristic systemic model of the element, and a produced radon progeny following the modified systemic model of the element.

The compartments explicit to the systemic model of a parent radionuclide are assumed by ICRP to be part of the systemic compartment 'other' of the daughter. This is the guideline used in the 'Occupational Intakes of Radionuclide' (OIR) series of ICRP. As an example, to consider the removal and uptake of polonium in the compartment 'fat 1', explicit to radon, ICRP has divided the compartment 'other' into two parts 'other*' and 'fat 1'. Based on this

approach, the sum of transfer rate from ‘plasma’ to ‘other*’ and ‘plasma’ to ‘fat 1’ is equal to the transfer rate from ‘plasma’ to ‘other’, i.e.

$$T(plasma \rightarrow other*) + T(plasma \rightarrow fat\ 1) = T(plasma \rightarrow other).$$

where the transfer rate ‘plasma’ → ‘fat 1’, is based on the mass fraction of ‘fat 1’ with respect to ‘other’. To illustrate:

$$T(plasma \rightarrow other*) = 0.9\ d^{-1}$$
$$T(plasma \rightarrow fat\ 1) = 0.1\ d^{-1}$$
$$T(plasma \rightarrow other) = 1\ d^{-1}$$

assuming 10% of mass fraction of ‘other’ is associated with ‘fat 1’. Solving the first order differential equations results in the same number of radioactive decays in ‘other’ and ‘other*’ + ‘fat1’. The modified and characteristic systemic model of the element are on this basis the same (D. Gregoratto, personal communication, October 30, 2023). Therefore, the inhaled radon progeny were allowed to follow the modified systemic model of its element.

2.2. Deposition of particles in the human respiratory tract regions

Initially, the depositional fractions of Table F. in ICRP Publication 66 were considered for use for the unattached and attached radon progeny. The table presents depositional fractions for log-normal aerosol size distribution and for each type of physical activity, defined as sleeping (resting), sitting, light exercise and heavy exercise. Later in the process, the work of Klumpp and Bertelli (Klumpp & Bertelli, 2017) was discovered, where the authors have produced depositional fractions of the respiratory tract regions (ET_1, ET_2', BB', bb' and AI) of ICRP Publication 130 for ‘mixed activity’, that is combination of the previously mentioned singular physical activities. The depositional fractions are valid for standardized time distribution spent on each singular physical activity for the typical member of the public of different age and sex, who is nose-breather. The standardized time distributions have been collected from ICRP Publication 71 (1995). For this work, the depositional fractions obtained by Klumpp and Bertelli have been utilized, to broaden the applicability of the results, thereby not limiting the results to only one specified singular activity.

As previously described in section 1.3. Background, the unattached radon progeny follows a unimodal activity size distribution. To take this fact into account, the value of the unattached radon progeny was described as a probability density function, with lower and upper diameter threshold of 0.5 nm and 10 nm, respectively, according to previous studies (Porstendörfer, 1994, 2001). The trimodal activity size distribution of attached radioactive progeny has been measured by Porstendörfer (2001) for indoor environments without additional aerosol particles, like cigarette smoke and cooking. The study resulted in no coarse mode, explained by the greater rate of plate out, i.e. deposition of the aerosols on surfaces. The lower and upper particle size threshold for nucleation and accumulation mode, applied in this work, have been estimated from graphs produced by Porstendörfer (2001).

Probabilistic size distribution calls for a necessity to derive continuous polynomials describing the depositional fractions as a function of lognormally distributed particle sizes. The polynomials were optimized for unattached mode, nucleation mode and accumulation

mode. In some cases, the same polynomial was estimated as adequate to describe the nucleation and accumulation mode. The extracted polynomials are tabulated in Appendix C: Polynomials describing fractional deposition in the lung regions, for members of the public of different age and sex.

Table 2 shows the input parameter values in this study. The fraction f, of the aerosols that typically exists in a certain mode is described in terms of potential alpha energy concentration (PAEC). PAEC is defined as the sum of alpha energy emitted from the decay of all the short-lived radon progeny in a volume of air (ICRP, 2014). The unattached fraction is based on values published by Porstendörfer (1994). The parameter values for attached fractions are based on published values for workplaces in ICRP Publication 137 (2017), since the results for workplaces are based on measurements in homes and workplaces.

Table 2. Aerosol parameter values for home exposure to ^{222}Rn-progeny. AMTD = activity median thermodynamic diameter. σ = geometrical standard deviation and f_p = fraction in terms of potential alpha energy concentration for the different modes. Indices u, n and a stand for unattached, nucleation and accumulation mode. The name 'unattached mode', which is the same as 'cluster mode', is here used for consistency with the parameter values defined in the Ecolego-model.

Unattached mode			**Nucleation mode**			**Accumulation mode**		
$AMTD_u$	$\sigma_{g,u}$	$f_{p,u}$	$AMTD_n$	$\sigma_{g,n}$	$f_{p,n}$	$AMTD_a$	$\sigma_{g,a}$	$f_{p,a}$
1 nm	1.3	0.1	30 nm	2.0	0.18	250 nm	2.0	0.72

The general default regional deposition fractions for gases, corresponding to 20% ET_2, 10% BB, 20% bb and 50% AI were applied for radon in this study (ICRP, 2015). Since radon is an inert gas, only a small fraction of the inhaled gas will remain after exhalation. This fraction was estimated by taking the ratio of the transfer coefficients for inhalation and exhalation and multiplying with the default values. The transfer rates for inhalation and exhalation were extracted from the study performed by Samuels et al. (2023).

In the systemic model for radon, all the depositional sites in the respiratory tract are described with only one compartment, namely respiratory tract air (RT-air). The value of the transfer rate from environment to the respiratory tract region is a function of the value of the transfer rate from RT-air to environment. RT-air is constituted of the volume fractions of the respiratory tract regions, which means that the transfer rate from environment could be multiplied with the regional volume fraction to get site-specific deposition. Assuming linear relationship between regional volume and regional mass, the masses of the respiratory tract regions were looked up in relevant ICRP Publications (ICRP, 2016, 2020). However, information on masses were incomplete regarding the regions BB and bb, hence the default regional deposition fractions were used.

Exposure to ionizing radiation can be divided into three categories: acute, continuous, and protracted exposure. The first exposure type has been applied here for simpler modelling approach. Replacement of acute intake with continuous intake would require considering the time varying accumulation and depositional pattern in the compartments of initial state,

thus introducing time as an additional independent variable in the study. Consideration of too many independent variables would increase the risk of disregarding the specific relationship between variables.

2.3. Simulation

The simulation settings were optimized for the specific dynamic model under study. This meant enabling the saturation option, since activity is a non-negative unit. 'Numerical Differentiation Formulas' was chosen as the solver used for simulation because the model includes radioactive chain of variable physical half-time, in addition to enable the software to use variable step size based on how much the activity in each compartment changes over time. The option 'Batch mode' was enabled and was set to 'one batch per decay chain' to decrease the simulation time. For the simulated output times, the option 'produce specified output only' was chosen as recommended by Ecolego for probability density functions to ensure the same time vector is returned for all iterations.

The simulation time, i.e. the time to track the activity in each compartment, was initially set to 365 days to be able to demonstrate the growth of the long-lived radon progeny in the different regions of the body. The simulation could however not be run through because of shortage of data capacity. The simulation time was therefore reduced in consecutive attempts to finally arrive at a simulation time of 1.5 days.

Four simulations were run. In each simulation, only one radionuclide (i.e. ^{222}Rn, ^{218}Po, ^{214}Pb and ^{214}Bi) was set to have an initial activity of 1 Bq/m^3. The doses from inhaled ^{214}Po are estimated to be negligible (Brudecki et al., 2014; Kendall & Smith, 2002) because of the radionuclide's short half-life. Therefore, no initial activity was set for ^{214}Po. Ingrowth of ^{214}Po from ^{214}Bi, i.e. ^{214}Po produced as decay product of ^{214}Bi on the other hand has been considered.

According to the manual of Ecolego, the cumulative activity can be obtained in the software. However, this feature could not be made viable. Therefore, the team behind Ecolego were reached for assistance. Meanwhile, tables over activity as function of time were converted from Ecolego to Excel-files (Microsoft Corporation) and were subsequently exported to MATLAB (R2022b, MathWorks, Natick, MA, USA). The area under the curve was calculated to acquire the cumulative activity.

The implemented biokinetic model was bench-marked against the software package Taurus, developed by UK Health Security Agency. Taurus uses the most recent biokinetic and dosimetric models of OIR series of ICRP Publications (ICRP, 2006, 2015, 2017) to calculate dose coefficients and for bioassay data (UKHSA, 2020, n.d.). The biokinetic model was evaluated through comparison of graphs over the time-varying activity in the lung, and corresponding Ã. Note: the lungs constitute of the source regions BB, BB_{seq}, BB_{bound}, bb, bb_{seq}, bb_{bound} and ALV.

2.4. Dosimetry of radon and radon progeny

The calculation of the S-coefficients would require more time than the time provided for the project. The calculation of absorbed dose in the target tissues of respiratory tract was

therefore performed in the free internal dosimetry program 'Internal Dose Assessed by Computer' (IDAC-Dose, version 2.1). IDAC-Dose is one of the programs used by ICRP Task group for calculating absorbed doses. The dose calculations are based on decay scheme data and SAF-values from Publications 107 and 133 respectively (Andersson et al., 2017). The SAF-values for preadults have not been officially published yet by ICRP, hence only doses for adult female and male are accessible. Another free dosimetry program is Dose and Risk Calculation (DCAL) programme (U.S. Environmental Protection Agency), through which SEE-values for all ages for members of the public can be extracted. However, the programme presumes sequential work manner, so that the biokinetics of the element need to be defined before SEE-values can be obtained. DCAL was created year 2006, ergo before the new revised biokinetic models were published. The revised changes in the models, in addition to assumed log-normally distributed particle sizes in this work, makes it impractical to use DCAL for purposes of this study.

IDAC-Dose 2.1 uses time-integrated activity coefficient a_{r_s}, as input for each source region of a user defined radionuclide. a_{r_s} is defined as

$$a_{r_s}(h) = \frac{\tilde{\mathrm{A}}_{r_s}}{A_0},$$

where $\tilde{\mathrm{A}}_{r_s}$ is the cumulative activity in the source region [MBq h] and A_0 is the initial inhaled activity [MBq].

The programme also generates effective dose, E (ICRP, 2007). Effective dose is a radiation protection quantity that takes into account the radiation sensitivity of different body organs and tissues, expressed as tissue weighting factors, w_T. The tissues weighting factors are based on data on both females and males and are therefore averaged over both sexes. Contribution from each organ and tissues to the total detriment is reflected from the value of w_T. The sum of w_T over all organs and tissues that are believed to contribute to stochastic effects is 1. Effective dose is defined as:

$$E\ (Sv) = \sum_T w_T \sum_R \frac{w_R D_R(r_T, T)_{ref.\ male} + \ w_R D_R(r_T, T)_{ref.\ female}}{2},$$

where the mean absorbed dose are over reference male and female in the target region r_T that contribute to stochastic effects (Andersson et al., 2017). w_R is the radiation weighting factor, accounting for biologic effects of radiation type R (Isaksson, 2017).

The programme has incorporated source region 'other' based on the characteristic biokinetic model of different elements. 'Other' needs to be an identifiable anatomical tissue, since the SAF($r_T \leftarrow r_{other}$) takes into consideration the masses of organs and tissues included in 'other'. To note, IDAC-Dose is developed for diagnostic nuclear medicine, hence decay products produced inside the body are not considered. Therefore, in the calculation of the SAF for the source region 'other', the programme subtracts the SAF-values of the included source regions in the characteristic biokinetic model to generate the SAF-value for 'other' (Andersson et al., 2017). Out of the short-lived radon progeny, only polonium has a source region 'other' that can be directly used for dose calculation in IDAC-Dose 2.1. For this case,

the cumulative activity from the added compartments (of fat and breast for taking account of polonium as progeny of radon; trabecular bone volume and cortical bone volume as progeny of lead) were summed with the cumulative activity of 'other'. For lead and bismuth, the added compartments were separately considered, since their associated soft tissues compartments are based on biokinetics and are not anatomically identifiable tissues. The systemic source regions for the different elements are shown in Table 3. The source regions in respiratory and alimentary tract are mutual between the elements.

Table 3. Systemic source regions of radon and radon progeny. The underlined source regions are part of 'other' in the characteristic biokinetic model for polonium.

Rn	**Po**	**Pb**	**Bi**
Blood	Blood	Blood	Blood
RT-air	RT-air	RT-air	RT-air
Adipose	Adipose	Adipose	Adipose
Breast	Breast	Breast	Breast
CB-volume	CB-volume	CB-volume	CB-volume
TB-volume	TB-volume	TB-volume	TB-volume
Red marrow	CB-surface	CB-surface	CB-surface
Liver	TB-surface	TB-surface	TB-surface
Kidneys	UB-content	UB-content	UB-content
Yellow marrow	Spleen	Spleen	Spleen
Other	Skin	Skin	Skin
	Gonads	Gonads	Gonads
	Red marrow	Red marrow	Red marrow
	Liver	Liver	Liver
	Kidneys	Kidneys	Kidneys
	Yellow marrow	Yellow marrow	Yellow marrow
	Other		

2.4.1. Calculating effective dose

The effective dose was calculated from the model, to evaluate the performance of the biokinetic model more comprehensively. Initially, an annual effective dose was calculated for comparison with obtained values by Kendall & Smith (2002). However, different factors between the two studies, such as the structure of the biokinetic models and differences on the absorption parameter values made the comparison quite impracticable. Therefore, another approach was used for calculation of effective dose.

The effective dose per exposure to airborne short-lived radon progeny is usually expressed per Working Level Month (WLM) (ICRP, 2017). WLM is defined as any combination of radon progeny in 1 m^3 of air that will emit $20.8 \cdot 10^{-6}$ J potential alpha energy, cumulated for a working month of 170 hours (ICRP, 2010).

The effective dose per WLM is defined as follows:

$$E\ (mSv\ per\ WLM) = \sum_{j=1}^{3} f_{pj} \sum_{i=1}^{3} I_{j,i}\ e_{j,i}.$$

The index j is for the mode of activity size distribution, that is j = 1, 2, 3 corresponds to unattached mode, nucleation mode and accumulation mode, respectively. The index i stands for the inhaled radon progeny, with i = 1, 2, 3 corresponding to ^{218}Po, ^{214}Pb and ^{214}Bi. The term f_{pj} is the fraction of PAEC associated with a certain mode j. $I_{j,i}$ is the inhaled radon progeny of mode j and type i. $e_{j,i}$ is the effective dose coefficient (Sv per Bq) of mode j and radon progeny i. For simplicity only contribution from ^{218}Po and ^{214}Po with α-particle energies of 6.11 and 7.83 MeV respectively were considered and calculated with IDAC-Dose 2.1. The effective dose coefficients were produced for a commitment period of 1.5 days and were calculated for the conditions specified in Table 2 in IDAC-Dose 2.1. For example, the time-integrated activities from the simulation corresponding to initial air concentration of ^{218}Po = 1 Bq/m^3, was used to obtain effective dose from ^{218}Po and ^{214}Po in unattached, nucleation and accumulation mode. The effective doses from ^{218}Po and ^{214}Po were summed together to obtain effective dose coefficient for ^{218}Po in unattached, nucleation and accumulation mode.

Intake of a radon progeny of type i, is given by:

$$I_i\ (Bq) = \ C_i\ t\ B,$$

where C_i is the air activity concentration of the radon progeny type i giving 1 WLM (Bq/m^3), t is 170 hours and B is the breathing rate (m^3/h) (ICRP, 2017). For an adult male, the dominating physical activity during a typical day is attributed to light exercise, giving a breathing rate of 1.5 m^3/h (ICRP, 1995). The same breathing rate was assumed for female. The concentration of mixed radon progeny giving 1 WLM is given in Table 4.

Table 4. Concentration of mixed radon progeny corresponding to 1 WLM. Values are extracted from table A.9 of ICRP Publication 137 (ICRP, 2017).

Radon progeny nuclide	**Activity concentration (Bq/m^3)**	
	Unattached mode	Attached mode
^{218}Po	$2.41 \cdot 10^4$	$5.21 \cdot 10^3$
^{214}Pb	$2.41 \cdot 10^3$	$3.91 \cdot 10^3$
^{214}Bi	-	$3.13 \cdot 10^3$

2.4.2. Study of doses to respiratory tract regions for an arbitrary condition

In radiation protection, the doses at reference level (=200 Bq/m^3 - residual air concentration of radon in Sweden) are of specific interest, hence chosen as the air concentration of ^{222}Rn.

As mentioned in section 2.4.1., initially an annual effective dose was calculated in accordance with air parameter values used by Kendall & Smith (2002) for 200 Bq/m^3 radon concentration in air. To be efficient in terms of time, the associated annual absorbed doses were used for study of dose distribution in respiratory tract regions. The dose calculation involved the following steps. The obtained Ã for 1 Bq/m^3 inhaled radon, inhaled radon progeny and their associated decay products produced inside the body, were scaled by 7300 m^3 which is the annual air volume inhaled by an adult male (Kendall & Smith, 2002). The air activity concentration of radon and its chain members depend on composition and

behaviour of air such as number concentration of trace gases, turbulence in air and size distribution of aerosols (Porstendörfer, 2001). For this study, the ratio of activity concentration between radon and radon progeny, corresponding to an equilibrium factor of 0.41, was assumed as follows:

1: 0.9: 0.45: 0.225

for the radioisotopes ^{222}Rn: ^{218}Po: ^{214}Pb: ^{214}B. The dose calculation for inhaled radon progeny of type i and the progeny as decay product of an inhaled parent radionuclide were handled separately in IDAC-Dose 2.1. For example, in IDAC-Dose, the initial activity was set to 200 Bq for ^{222}Rn, to obtain the annual absorbed dose and effective dose for this specific initial activity. The source regions used for dose calculation included those inside and outside of respiratory tract.

2.5. Integration of biokinetics and dosimetry in Ecolego for direct access of absorbed doses for an initial set of deposition conditions

Late in the project, the error causing unfeasible extraction of cumulative activity in the software (Ecolego) was found and solved. In addition, the S-coefficients were decided to be incorporated in Ecolego for direct access of absorbed doses for an initial set of deposition conditions such as aerosol size, air concentration of the radionuclides, fraction associated with each activity size distribution of attached radon progeny etc.

The majority of the short-lived radon progeny decay at the deposition sites before clearance takes place (Harrison, 2009). Therefore, for simplicity in dose calculations, the source regions were narrowed to constitute of those only contained in the lungs (i.e. BB, BB_{seq}, BB_{bound}, bb, bb_{seq}, bb_{bound} and ALV). The SAFs of adult male and adult female were interpolated from electronic data files of ICRP Publication 133, with respect to the mean energies of the emitted particles given in Table 5. The extracted SAFs were then multiplied with the Δ-values given in Table 6. The values of Table 5 and Table 6 were extracted from the supplementary DECDATA software of ICRP Publication 107. Furthermore, the contribution from β-emission was approximated with the mean energy of the emitted particle, instead of integrating over the β-spectrum.

Table 5. Mean energies ($E_{i,R}$) in MeV for emitted particles during the decay of radon and short-lived radon progeny. The values are from supplementary material, DECDATA software, of ICRP Publication 107 (2008).

Radionuclide	Auger electrons	Conversion electrons	β-radiation	α-particles	α-recoils
^{222}Rn	9.16E-4	4.41E-1		5.489	1.0E-1
^{218}Po			7.14E-2	6.002	1.12E-1
^{214}Pb	8.13E-4	1.64E-1			
^{214}Bi	9.34E-4	8.16E-1	6.41E-1	5.46	1.04E-1
^{214}Po	8.83E-4	7.01E-1		7.687	1.47E-1

Table 6. Absorbed dose rate (Δ), expressed in Gy kg Bq^{-1} s^{-1} for radon and short-lived radon progeny. The values were extracted from supplementary material, DECDATA software, of ICRP Publication 107(2008).

Radionuclide	Auger electrons	Conversion electrons	β-radiation	α-particles	α-recoils
^{222}Rn	3.70E-20	1.67E-18		8.80E-13	1.62E-14
^{218}Po			2.29E-18	9.62E-13	1.80E-14
^{214}Pb	6.89E-16	1.16E-14			
^{214}Bi	4.30E-17	3.47E-15	1.03E-13	1.84E-16	3.50E-18
^{214}Po	1.82E-21	1.30E-19		1.32E-12	2.35E-14

The statistical uncertainty of the absorbed doses was calculated by taking the square root of the sum of the variance of constituent terms. Variances were extracted from Ecolego.

3. Results

Figure 7 presents the sub-systems of the biokinetic model and attainable absorbed doses for inhalation of radon and radon progeny. The sub-systems 'HRTM initial', 'Transport state' and 'Bound state' contain the compartments of HRTM. The sub-systems 'HATM' and 'systemic model' in turn contain all compartments of associated models. 'Source region' constitute of aggregate blocks, summing the activity from compartments situated in different sub-systems that are associated with one source region. The sub-system 'cumulative activity' gives corresponding values for combinations of 1) radon and radon progeny, 2) different modes of activity size distribution of radon progeny in air, 3) for members of the public of ages 3 months old, 1 year old, 5 years old, 10 years old, 15 years old and adults defined by ICRP and 4) gender for 15 years old and adults. The sub-system 'electron dose' gives electron doses from ^{214}Pb and ^{214}Bi that predominantly decay by β-emission. The sub-system 'alpha dose' gives alpha doses from ^{222}Rn, ^{218}Po and ^{214}Po which dominantly decay by α-emission. The total contribution from the emitted particles presented in Table 5 can be obtained from the sub-system 'absorbed dose' for adult male and female.

The right-hand side of the figure contains parameters for transfer coefficients between compartments, initial air concentration of radon and radon progeny, fraction attributed to each activity size distribution and aerosol size for easy access and model-management. For example, the parameter 'PRO' contains all transfer coefficients that need to be introduced to take account of progeny produced inside the body. The parameters u, n, and a correspond to the particle size for unattached radionuclides and the radionuclides in nucleation and accumulation mode, respectively. f_u, f_n_ and f_a correspond to the fractions associated with unattached mode, nucleation mode and accumulation mode, respectively. The initial air activity concentration of a specific radionuclide is the input value of the radionuclide in question.

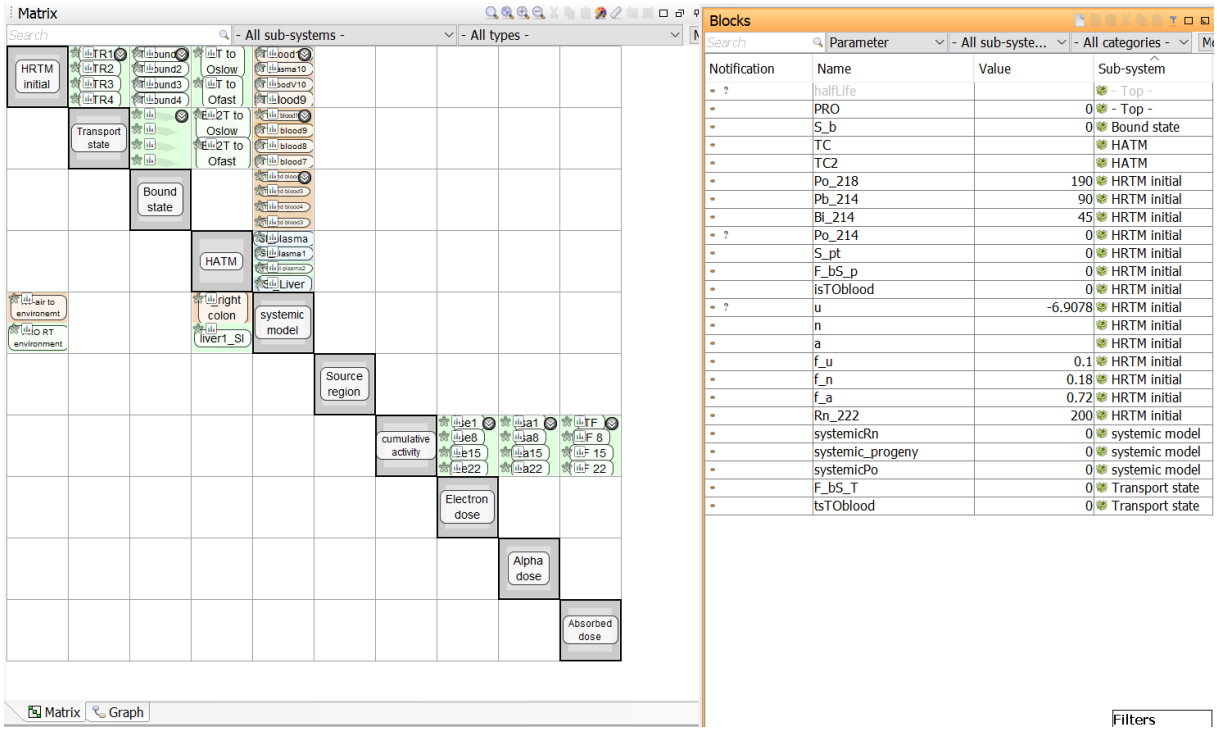

Figure 7. The sub-systems of the biokinetic model describing the movement of radon and radon progeny inside the body. Each sub-system constitutes associated compartments. The last three sub-systems in the matrix give electron dose, alpha dose and total contribution of electron and alpha dose. The right-hand side of the figure depicts the parameters for transfer coefficients, initial air activity concentration, particle size of unattached, nucleation and accumulation mode that can be set as probabilistic and associated fraction.

Table 7 compares the obtained Ã from the present work and Taurus for 5 µm aerosol size, f_a = 1, adult male and 'light work', defined as singular activity in Taurus. The Ã obtained directly in Ecolego were similar to calculated Ã with MATLAB. Ã for a specific radionuclide is derived from both the inhaled radionuclide in question and those that have been produced inside the body. From the relative bias, it is noticed that Ã from ^{222}Rn is underestimated by 99.3 %. For ^{218}Po, a comparatively smaller Ã was obtained, that deviates with 19.9%. For other radon progeny the discrepancies lie under 19%.

Table 7. Obtained cumulated activity in the lung, compared to corresponding values obtained with the software package Taurus. As an example, Ã for ^{214}Pb were extracted through summation of Ã following inhalation of ^{214}Pb and from ^{214}Pb as decay product of ^{218}Po and ^{222}Rn. The Ã have been obtained for 5 µm aerosol size, f_a = 1, adult male, 'light work' as defined singular physical activity in Taurus and an integrated time of 1.5 days. Lung as a whole source region includes the constituent source regions BB, BB$_{seq}$, BB$_{bound}$, bb, bb$_{seq}$, bb$_{bound}$ and ALV.

Radionuclide	*Ã [Bq h]*		*Relative bias*
	Present work	Taurus	
^{222}Rn	0.0000720	0.00989	-99.3 %
^{218}Po	0.00722	0.00902	-19.9 %
^{214}Pb	0.0631	0.0547	15.3 %
^{214}Bi	0.105	0.0884	18.9 %
^{214}Po	0.105	0.0884	18.9 %

Table 8 shows the effective dose from different dosimetric models including this work. As can be seen, the calculated effective doses range from 7–21.1 mSv/WLM. The value obtained in this study was 18.22 mSv/WLM, which is close to the produced values of Brudecki et al. (2014) and James et al. (2004) of 18 and 21.1 mSv/WLM respectively.

Table 8. Effective dose (mSv WLM^{-1}) for radon progeny from present and previous studies. The parameter values given in Table 2 were used for calculation of effective dose. Approach refers to the method or process used to assess the absorbed dose to the organs and tissues. In radiation protection, a dosimetric approach involves measurements, calculations or a combination of both to estimate the absorbed dose.

Effective dose (mSv WLM^{-1})	*Reference*	*Approach*
18.22	Present work	Dosimetric
21.1	James et al. (2004)	Dosimetric
11.5	Porstendörfer (2001)	Dosimetric
18	Brudecki et al. (2014)	Dosimetric
9.86	Zhu et al. (2018)	Dosimetric
7	Yu et al. (2001)	Dosimetric

Absorbed doses [mGy] from inhaled radon gas and radon progeny are shown in Table 9 for an annual air volume of 7300 m^3 and air activity concentration 200 : 190 : 90 : 45 Bq/m^3 for ^{222}Rn : ^{218}Po : ^{214}Pb : ^{214}Bi, calculated in IDAC-Dose. The difference in dose between male and female is quite small. The secretory cells of bronchial (BB_{sec}) were observed to attain higher absorbed dose than basal cells (BB_{bas}). Highest and smallest absorbed dose are to the secretory cells of bronchiolar (bb_{sec}) and the alveolar (ALV), respectively. It is also noted that absorbed doses from inhaled ^{222}Rn are approximately two orders of magnitude less than corresponding doses from inhaled radon progeny. The obtained doses in bb_{sec} and ALV are counter-intuitive between inhaled radon and inhaled radon progeny, which was an unexpected outcome. The bottom row of the table shows the obtained effective doses, which were 0.172 and 27.9 mSv for radon and radon progeny respectively.

Table 9. Obtained doses from inhaled radon gas and inhaled radon progeny using IDAC-Dose 2.1. Note: 'doses from radon gas' constitute of ^{222}Rn and its decay products. The doses have been calculated for the annual air volume inhaled, which is 7300 m^3, and air activity concentration 200 : 190 : 90 : 45 Bq/m^3 for ^{222}Rn : ^{218}Po : ^{214}Pb : ^{214}Bi. The aerosol parameter values given in Table 2 were used for calculation of absorbed doses and effective doses, for a commitment period of 1.5 days.

Target tissue	*Doses from radon gas [mGy]*		*Doses from radon progeny [mGy]*	
	Male	Female	Male	Female
BB_{bas}	0.0801	0.0642	9.2	8.61
BB_{sec}	0.325	0.259	18.6	17.5
bb_{sec}	0.0313	0.0233	19.2	21.4
ALV	0.00110	0.000993	0.780	0.902
Annual effective dose [mSv]	0.172		27.9	

Table 10 shows the calculated absorbed doses from inhalation of radon and radon progeny and their associated uncertainties that have been calculated using Ecolego. The absorbed doses from radon gas in the target tissues of bronchial airways are one order of magnitude smaller than corresponding values obtained using IDAC-Dose. For the remaining target tissues, the absorbed doses from radon and radon progeny lie in the same range for Ecolego and IDAC-Dose.

Table 10. Obtained doses from inhaled radon gas and inhaled radon progeny in Ecolego. Note: 'doses from radon gas' constitute of ^{222}Rn and its decay products. The doses have been calculated for the annual air volume inhaled, which is 7300 m^3, and air activity concentration 200 : 190 : 90 : 45 Bq/m^3 for ^{222}Rn : ^{218}Po : ^{214}Pb : ^{214}Bi. The aerosol parameter values given in Table 2 were used for calculation of absorbed doses for a commitment period of 1.5 days.

Target tissue	*Doses from radon gas [mGy]*		*Doses from radon progeny [mGy]*	
	Male	Female	Male	Female
BB_{bas}	$0.00834 \pm 1.63 \cdot 10^{-8}$	$0.00625 \pm 1.53 \cdot 10^{-8}$	9.19 ± 3.09	6.95 ± 2.13
BB_{sec}	$0.0388 \pm 3.0 \cdot 10^{-8}$	$0.0294 \pm 2.82 \cdot 10^{-8}$	19.7 ± 6.09	18.8 ± 1.52
bb_{sec}	$0.0404 \pm 5.58 \cdot 10^{-10}$	$0.0297 \pm 2.82 \cdot 10^{-10}$	22.4 ± 4.16	25.0 ± 4.62
ALV	$0.00103 \pm 2.15 \cdot 10^{-11}$	$0.000889 \pm 2.11 \cdot 10^{-11}$	0.87 ± 0.13	0.972 ± 0.158

Table 11 presents target tissue absorbed doses [mGy] in thoracic region from the dominating decay mode of the short-lived radon progeny for adult female and male. The absorbed doses are obtained for an annual inhaled air corresponding to 7300 m^3 and air activity concentration of 190 : 90 : 45 Bq/m^3 for ^{218}Po : ^{214}Pb : ^{214}Bi.

Table 11. Doses from the dominating decay mode (i.e. α or β) of the inhaled radon progeny using IDAC-Dose 2.1. The doses are calculated for annual inhaled air of 7300 m^3, and for air activity concentration of 190 : 90 : 45 Bq/m^3 for ^{218}Po : ^{214}Pb : ^{214}Bi. The parameter values given in Table 2 were used for calculation of absorbed doses from α- and β-particles, for a commitment period of 1.5 days.

Target tissue	*α-/ β-doses from inhaled radon progeny [mGy]*				*Gender*
	^{218}Po (α)	^{214}Pb (β)	^{214}Bi (β)	^{214}Po (α)	
BB_{bas}	0.186	0.168	0.179	8.65	Male
	0.190	0.153	0.175	8.08	Female
BB_{sec}	1.68	0.210	0.201	16.5	Male
	1.70	0.191	0.195	15.4	Female
bb_{sec}	1.71	0.147	0.144	17.2	Male
	1.90	0.162	0.153	19.2	Female
ALV	0.0482	0.0251	0.131	0.637	Male
	0.0560	0.03	0.136	0.733	Female

4. Discussion

4.1. Biokinetic model

From Table 7, the cumulated activity of radon gas is underestimated by two orders of magnitude in comparison to Taurus. Upon inspection of the graphs depicting activity as a function of time, it is likely that Taurus treats the entire inhaled radon gas to be deposited in respiratory tract regions. This contrasts with the biokinetic model implemented, in which the quotient of transfer rate from inhaled and exhaled radon gas was considered to be deposited. Furthermore, focusing on the sign of relative bias for a moment, ^{218}Po is shown to be the only radon progeny with smaller Ã than Taurus. This may be because the total Ã only stem from the inhaled radon progeny itself and as decay product of ^{222}Rn which is very small. For the remaining chain members, daughters from preceding radionuclides contribute with the total Ã.

The breathing parameters attributed to different physical activities determine the deposition efficiency (see Appendix C for polynomials describing depositional fraction in respiratory tract regions). The extracted activities from Taurus are true for light work. Comparison of activities at the initial time showed that deposition is overestimated by approximately 20% for all inhaled radon progeny in the implemented model, therefore being a possible explanation to the differences in obtained Ã.

Initially, the biokinetic models were designed in the compartment modelling computer programme ‘Simulation, Analysis And Modelling software’ (SAAM) II (version 1.1, Nanomath, US). The main advantage of the software is that it is user friendly. The main crucial limitation on the other hand was thought to be the inability to assign transfer coefficients to describe deposition in the sequestered compartments of respiratory tract, expressed in percentage. Therefore, the biokinetic models were redesigned in Ecolego, wherein the same challenge was later discovered to also be present but was solved through writing equation to describe initial deposition in the compartments of discussion. In other words, other software, such as SAAM II, might be an alternative software for construction of the compartment model. However, doses obtained through Ecolego are shown to be more accurate in comparison to corresponding values obtained through SAAM II (Bengtson, 2018). The reason behind this was thought to be the different types of ODEs solvers that are used to solve the differential equations, which through analysis of the documentations on the software packages seems to hold true (Barrett et al., 1998; Ecolego, 2023). Through the years, SAAM II has continued to use the same ODEs solvers, with the main difference that the solvers have been developed to be more stable in handling stiff problems (Nanomath, personal communication, February 12, 2024).

For the purposes of this study, Ecolego is suggested as a more appropriate tool to use for modelling of the biokinetics of radon and radon progeny. The ability to directly assign age-, sex-, and radioisotope specific transfer coefficients, eliminate the need for different multi-compartment model for each reference member of the public and radioisotope, hence construction of the biokinetic model is less complex. In addition, the software enabled defining initial aerosol sizes as probabilistic entities and run probabilistic simulations on

these, which is thought to improve the accuracy of the results. Moreover, the possibility of further processing of Ã was available for dose calculation.

Returning to the subject about probabilistic simulations, initial deposition of unattached radionuclides was discovered to output negative values in a few deposition regions, for some members of the public. Multiple attempts were made to adjust the polynomials corresponding to unattached mode, but no effective results could be obtained for all groups of people of different age and sex. For consistency, the polynomials were therefore replaced with the deposition fraction corresponding to 1 nm unattached radionuclide for all members of the public and were consequently represented as deterministic simulations.

4.2 Dosimetry

As can be seen from Table 8, the effective dose calculated from the biokinetic model falls within the range of effective dose calculated by other researchers. The difference between obtained values attribute to values on the factor on breathing parameter(s), aerosol particle size, fraction of unattached and attached radionuclides. Brudecki et al. (2014) have for example taken account of trimodal activity size distribution of radon progeny and used indoor mixed physical activities. Zhu et al. (2018) treated inhaled radon progeny as unattached or attached and used a breathing rate value of 0.54 m^3/h.

From Table 9, the annual effective dose from radon and radon progeny sum to 28 mSv, which is 1.4 times greater than the value obtained by Kendall & Smith (2002). Harrison and Marsh (2020) calculated an annual effective dose of 14 mSv at 300 Bq/m^3 radon concentration for an annual home occupancy of 7000 hours, which corresponds to 9.3 mSv at 200 Bq/m^3. The value obtained in present work is by comparison three times greater than the reported value by Harrison and Marsh. The differences on obtained values between the studies may lie in the approached methodology and parameter values used for calculation of annual effective dose.

The second aim of the study was to analyse the absorbed doses between respiratory tract regions. For this purpose, the discussion on dosimetry concentrates on obtained doses using IDAC-Dose, since they provide validated values. The calculated absorbed doses in Table 10 are based on approximative values of total energy deposited in the target regions and can be perceived more as a demonstration of the ability to do dose calculations and associated uncertainties in the software. The absorbed doses obtained in Ecolego are in the range of the values calculated with IDAC-Dose; with absorbed doses in the target tissues of bronchial airways from inhaled radon gas as an exception which is discussed in the next paragraph. Care was taken while calculating the S-coefficients to generate accurate values. However, errors may have arisen during the calculation process.

A distinct difference between the absorbed doses using Ecolego and IDAC-Dose is on the obtained bronchial doses from radon gas, where Ecolego gave doses about ten times smaller than corresponding values using IDAC-Dose. The results were ambiguous since no clear pattern could be observed upon comparison to the bronchial doses from inhaled radon progeny. The differences are not either caused by incorporated S-coefficients since they influence the absorbed doses from radon gas and radon progeny to approximately the same

degree. The only difference is that absorbed doses from radon gas also do take S-coefficients for ^{222}Rn into account. Hence, potential causes are rather difficult to point out.

Previous investigations (Winkler-Heil et al., 2007; Zhu et al., 2018) show that a high deposition in a respiratory tract tissue correlates with a high dose in that specific tissue, with AI as an exception which is discussed later. For both unattached and attached radon progeny, the greatest proportion of the fraction is deposited in the ET airways (Kendall & Smith, 2002). One surprising outcome from Table 9 was the contrary doses in bb_{sec} between male and female from radon gas and radon progeny. The mass of the target tissue is the same for both genders (ICRP, 2016). Table 12 shows deposition fraction in respiratory tract regions. Pattern of deposition fraction in bb are consistent with obtained doses in bb_{sec}.

For ALV, the difference in absorbed doses between radon gas and radon progeny are rather difficult to interpret. The mass of ALV is smaller for females, therefore it seems more likely to acquire a higher absorbed dose in comparison to males.

Table 12. Deposition fraction from inhaled radon gas and radon progeny in respiratory tract regions for adult females and males. The depositional fractions were calculated with the polynomials of Table 22 and Table 23, and have been obtained for parameter values of Table 2. Furthermore, the fractions are valid for 1 Bq/m^3 initial air concentration of radon and only one radon progeny (here ^{218}Po), since the deposition site is insensitive of the type of radon progeny (i.e. ^{218}Po, ^{214}Pb or ^{214}Bi).

Deposition region	**Radon gas**		**Radon progeny**	
	Male	Female	Male	Female
ET_1			$1.01 \cdot 10^{-1}$	$1.04 \cdot 10^{-1}$
ET_2	$7.78 \cdot 10^{-4}$	$6.19 \cdot 10^{-4}$	$5.58 \cdot 10^{-2}$	$5.70 \cdot 10^{-2}$
BB	$3.89 \cdot 10^{-4}$	$3.09 \cdot 10^{-4}$	$1.67 \cdot 10^{-2}$	$1.52 \cdot 10^{-2}$
bb	$7.78 \cdot 10^{-4}$	$6.19 \cdot 10^{-4}$	$4.48 \cdot 10^{-2}$	$4.78 \cdot 10^{-2}$
ALV	$1.95 \cdot 10^{-3}$	$1.55 \cdot 10^{-3}$	$1.52 \cdot 10^{-1}$	$1.44 \cdot 10^{-1}$

Absorbed and effective doses from inhaled radon gas were shown to be about two orders of magnitude smaller than corresponding doses from inhaled radon progeny, in accordance with previous studies (Hofmann et al., 2012; Kendall & Smith, 2002). Consistent with paper by Hofmann et al. (2012) about 95% of effective dose is attributed to absorbed doses in lungs. Effective dose calculated from absorbed dose in lungs and body organs outside thoracic tissues was 0.172 mSv. Effective dose from only lung dose was calculated to 0.165 mSv, which is about 5% smaller.

Turning to doses from radon progeny, the presented deposition fraction reflects those of Zock et al. (1996) and Mohamed (2004), who found that the deposition fraction increases further down the thoracic respiratory tract airways, i.e. from BB to AI, for increasing particle sizes. However, the results show that the doses will be higher in BB and bb, rather than AI. The reason behind this may lie in the masses of the target tissues. The target tissue of AI has a mass about three orders of magnitude greater than the target tissue masses of BB and bb (ICRP, 2016), causing the comparably higher tissue dose.

The geometrical distance between source region and target region is important for traversal of the energized short ranged α particles that are deposited on mucous layer in bronchial and bronchiolar airways. Depending on the depth of the target tissues, the doses vary accordingly. On this note, the secretory cell layer of bronchial will receive higher dose than the basal cell layer.

The secretory cells of bronchiolar airways were found to get highest absorbed doses in the lungs, even though they have a larger mass than bronchial secretory cells. There are two possible causes. bb_{sec} is the only target tissue in bronchiolar airways, so that all deposited energies from source regions in bronchiolar will accumulate in one tissue only. The second cause may be due to the deposition pattern, where bb has higher deposition fraction than BB.

From the presented results on absorbed doses from α- and β-emission particles from short-lived radon progeny in Table 11, it was observed that emitted α-particles give rise to the highest doses. The high α-energy of ^{214}Po (7.83 MeV compared to 6.11 MeV for ^{218}Po), in addition to the fact that it can be produced from three parent radionuclides, makes its contribution to absorbed dose the highest. The α-particle of ^{214}Po has a continuous slowing down approximation (CSDA) range of 76 µm (in skeletal muscle), which means the emitted energy is absorbed locally with respect to decay site (NIST). Furthermore, the intrinsic characteristic of ^{214}Pb to chemically bind to respiratory tract airway walls, result in more decays to happen from ^{214}Pb and its decay products before clearance is completed. To illustrate the difference of α-doses in bronchial airways between these two isotopes, the α-dose from ^{218}Po following inhalation of 1 Bq ^{218}Po, and ^{214}Po following inhalation of 1 Bq ^{214}Bi, was calculated in IDAC-Dose. The results are shown in Table 13.

Table 13.The α-doses [mGy] in the target tissues of bronchial airways from the decay of ^{218}Po following inhalation of 1 Bq ^{218}Po, and ^{214}Po following inhalation of 1 Bq ^{214}Bi. The doses are valid for adult male and have been calculated with IDAC-Dose for higher accuracy. The cumulative activities were extracted from the Ecolego-model. The values were obtained using deterministic simulation, with parameter values according to Table 2.

Target tissue	**^{218}Po**	**^{214}Po**
BB_{bas}	$9.34 \cdot 10^{-8}$	$1.62 \cdot 10^{-6}$
BB_{sec}	$8.47 \cdot 10^{-7}$	$3.25 \cdot 10^{-6}$

The property of local absorption becomes clearer through comparison of doses between BB_{bas} and BB_{sec} for ^{218}Po, ^{214}Pb and ^{214}Bi that have dominating decay mode of α-, β- and β-emission respectively. The comparatively shorter CSDA range of 48 µm (in skeletal muscle) for ^{218}Po-α gives significantly higher doses in BB_{sec} that are situated nearer the source particles. A much smaller fraction of α-energy is deposited in BB_{bas}. The differences in dose are less prominent for ^{214}Pb-β and ^{214}Bi-β with CSDA ranges of 844 µm and 2790 µm (in soft tissue), respectively (NIST).

Overall, the estimated doses are valid for the reference member of the public, who is non-smoker under normal aerosol conditions measured in Germany (Klumpp & Bertelli, 2017; Porstendörfer, 2001). For environments with additional aerosols from smoking or cooking, the activity size distribution is shifted towards greater aerosol sizes (Porstendörfer, 2001).

The exclusion of nucleation mode will for example decrease the absorbed dose by the fraction radon progeny associated with nucleation mode. An increase in aerosol concentration in air will lead to higher attachment rate, signifying a decrease in unattached fraction radon progeny (Porstendörfer, 1994). Similarly, the total dose will decrease by the reduce in unattached fraction.

Darby et al. (2005; 2006) conducted a meta-study analysing the individual data from 13 European case-control studies. The study found that the relative risk for lung cancer when exposed to radon is the same for non-smokers and smokers. On the other hand, the cumulative absolute risk of death from lung cancer at the age of 75 years is about 25 times greater for smokers than lifelong non-smokers. The results obtained in this study are valid for non-smokers. However, based on previous studies (Baias et al., 2009; Darby et al., 2005; 2006), the results need to be handled carefully for populations other than non-smokers.

In Baias et al. (2009) comparative study on doses for four categories of smokers: 1) light, short-term (LST) smokers, 2) light, long-term (LLT) smokers, 3) heavy, short-term (HST) smokers and heavy, long-term (HLT) smokers, it was found that the doses will deviate minimally for LST smokers because of very small morphological and physiological smoke-induced changes. For HST and LLT smokers, the doses will decrease because of higher mucociliary clearance, in addition to the thickening of the mucus layer, resulting in reduced fraction of decay energy reaching the target cells. In contrast, for HLT smokers, an increase in doses were observed caused by impaired mucous clearance velocities, higher breathing frequency, morphological changes in lung tissues and smoke-induced lung diseases.

The lung doses for preadults could not be calculated because of unpublished S coefficients by ICRP. The doses for children might however lie in the same range as those for adults in accordance with previous reports (Hofmann et al., 2012; ICRP, 2010; Kendall & Smith, 2005), because of simultaneous competing mechanisms. Children have lower ventilation rate, which decreases the amount of activity inhaled, while the lighter target tissue masses increase the doses. Similarly, the increased deposition by diffusion due to narrower airway diameters is cancelled out by shorter residence times in airway generations thereby reducing deposition. The use of varied parameter values across different research groups introduces uncertainties into dosimetry calculations. Upon reviewing the literature, the age-dependent parameters in dosimetry models can be said to consist of lung morphology like mass of target tissue through childhood to adulthood, diameter and length of airways, depth defined for target cells below epithelium and breathing parameters.

The obtained doses relate to the residential reference level (200 Bq/m^3) governed by the Swedish radiation safety authority (SSM). According to Rönnqvist (2021), about 330 000 small houses in Sweden are estimated to have an air concentration of radon exceeding the reference level. This corresponds to 16% of all Swedish small houses in 2021. Nearly 500 new cases of lung cancer are detected each year that are related to radon exposure. A specific work of note by Boice and John (2006) shows the relative risk of lung cancer and radon concentration to follow a dose-response relationship. Radon was confirmed as an apparent confounding factor to lung cancer at high radon concentration. The correlation was less evident below 150 Bq/m^3. In contrast, in the study by Darby et al. (2005; 2006), the relative risk of lung cancer was estimated to be linear with no threshold, for residential radon

concentration below 200 Bq/m^3. I would like to add that even though the results of the studies do not show consensus on the deleterious effects of radon at low concentrations, the risks can still not be ignored. Since every person inhale the ubiquitous radon with each breath, the small risks can translate into large number of diseases and lethality.

Naturally there exists sources of uncertainty in dose calculations. In this context, doses have been estimated for short-lived radon decay products, based on models that have primarily been developed with respect to longer-lived isotopes or stable isotopes. Different isotopes have different electric configuration, which influences the chemical interactions occurring within the body and thence the fate of the isotope. Small deviations in accuracy are consequently inevitable. Other reported uncertainties include among other:

- the aerosol activity size distribution considered;
- the breathing rate; and
- the model used for deposition in the respiratory tract (ICRP, 2010).

The capability to estimate doses based on probabilistically distributed aerosol sizes makes the estimated doses more relatable to actual doses a reference person is exposed to, compared to when calculations are based on deterministic aerosol diameters under the same environmental conditions. For a more accurate result, it is further needed to take account of factors such as hygroscopic property of the attached radon progeny, amounting to aerosol augmentation in the respiratory tract.

Absorbed dose is a macroscopic quantity that may not be sufficient to describe characteristics of energy deposition when radiosensitivity across target cells varies. Previous studies (Zhu et al., 2018) have reported dosimetric difference between regional models and bifurcation models. The dosimetry model of ICRP is based on a regional model, i.e. the characteristic depth of target tissues is defined for an infinite cylinder with average inner diameter based on the airway generations of the region. While in a bifurcation model, the characteristics of each generation are considered. Zhu et al. (2018) have developed a bifurcation model, which was suggested to be more suitable for internal dosimetry of short ranged α radiation.

4.3. Improvements

For more accurate values of absorbed doses, the values of S coefficients from source regions outside the respiratory tract can be incorporated in the software tool, i.e. Ecolego.

5. Conclusion

This study set out with the aim of implementing a biokinetic model in the software tool Ecolego, describing the movement of inhaled radon and radon progeny inside the body for members of the public. For a complete view of internal exposure, the human respiratory tract model, human alimentary tract model and systemic models presented by ICRP were integrated together, giving a multi compartment model. One of the strengths of the model is the use of Monte Carlo method to run probabilistic simulations with respect to normally

distributed attached radionuclides, increasing the accuracy of the results. The reconstructed model was bench-marked against Taurus through comparison of cumulative activities in the lungs, resulting in good agreement. To evaluate the performance of the entire biokinetic model, the effective dose for radon progeny was calculated from the model, giving consistent results with previous studies. A secondary aim of the study was to analyse the acquired absorbed doses from α- and β-radiation in the target tissues of the lungs. Validated values of absorbed doses were generated using the software IDAC-Dose 2.1. In addition, S coefficients from source regions inside the respiratory tract were incorporated in the software giving approximative values on absorbed doses and associated uncertainties. The differences in dose between respiratory tract regions were explained based on literature. The highest doses were shown to be from the energetic α-particles emitted by ^{218}Po and ^{214}Po, which are locally absorbed. Furthermore, it was discussed that the characteristics of deposited α-energies across different radiosensitive target cells may be better described using bifurcation models.

Acknowledgements

I would like to express my sincere gratitude to my supervisors, Mats Isaksson and Christopher Rääf, for their support and invaluable guidance throughout every stage of this project. A special thanks to Mats Isaksson for his insightful advice on the structure of the report and for patiently answering all my questions. I extend my thanks to Martin Andersson for his helpful responses regarding IDAC-Dose, which greatly aided me in overcoming various challenges. I would also like to thank Francisco Piñero García, Rimon Thomas, and Jonathan Sundström for their thoughtful contributions, which enriched different aspects of the project. Lastly, I am profoundly thankful to my family for their unwavering love, support, and encouragement, which has been my anchor throughout my academic journey.

Appendix A: Parameter values for transfer coefficients in HRTM and HATM

Table 14. Transfer coefficient between compartments in HRTM. Values for transfer coefficients were extracted from table A.1 of ICRP Publication 130 (2015).

From	To	Transfer coefficient [d^{-1}]
ET_1	Environment	0.6
ET_1	ET_2'	1.5
ET_2'	Oesophagus	100
ET_2'	ET_{seq}	0.2
ET_{seq}	LN_{ET}	0.001
BB'	ET_2'	10
BB'	BB_{seq}	0.2
BB_{seq}	LN_{TH}	0.001
bb'	BB'	0.2
bb'	bb_{seq}	0.2
Bb_{seq}	LN_{TH}	0.001
ALV	bb'	0.002
ALV	INT	0.001
INT	LN_{TH}	0.00003

Table 15. Age-specific transfer coefficients for total diet [d^{-1}] in the alimentary tract regions, given by table 6.6. in ICRP Publication 100 (2006). O=Oesophagus; ST = stomach; SI = small intestine; RC = right colon; LC = left colon; RS = rectosigmoid colon.

From	To	Transfer coefficient [d^{-1}]				
		3 months	1 year	5-15 years	Adult male	Adult female
O (fast)	ST-content	21 600	12 343	12 343	12 343	12 343
O (slow)	ST-content	2 880	2 160	2 160	2 160	2 160
ST-content	SI-content	19.2	20.57	20.57	20.57	15.16
SI-content	RC-content	6	6	6	6	6
RC-content	LC-content	3	2.4	2.182	2	1.5
LC-content	RS-content	2	2.4	2.182	2	1.5
RS-content	Faeces	2	2	2	2	1.5

Appendix B: Systemic models

B-1: Radon

The approached systemic model in this study is developed by Samuels et al. (2023) and is a refined version of the systemic model for radon described in ICRP Publication 137, developed by Leggett et. al (2013). The structure of the used systemic model for radon is

shown in Figure 8. The theoretical framework on which the model is based is explained in the remainder of the paragraph. Human volunteer studies have shown that ingested radon is easily absorbed into blood from the alimentary tract. Postulation on site/sites of absorption of radon gas is varied, where some investigators suggest absorption from both the stomach and the small intestine and others solely from the small intestine. The approached biokinetic assumes absorption from only the small intestine. The systemic model is simplified through pooling compartments that show similar time-dependent biokinetic behaviour of radon.

The presented systemic biokinetic model is simplified through eliminating pulmonary blood and dividing blood into arterial and venous compartments. The connection between arterial blood and venous blood is via a lung compartment, also known as respiratory tract (RT) air. Following inhalation of radon gas, most of the gas is exhaled. The rest is transferred to arterial blood, whence it travels to capillaries of systemic tissues, and continues to the venous blood and back to pulmonary blood in the RT-air where some of it is exhaled and the rest circulate once again. The cycle continues until the body burden is depleted. The retention time in each systemic tissue is determined by the radon solubility in the tissue and the blood flow to the tissue. As an example, for fat with a high radon solubility and poor blood flow, this implies high retention times. The radon solubility of a systemic tissue is represented with blood-to-tissue partition coefficient, which is defined as the ratio of the gas in blood and the compartment of interest at equilibrium. The values for partition coefficients are independent of age and sex. The assigned transfer coefficients are on the other hand age- and sex-specific and have been derived by Samuels et al. (2023).

Liver is the only systemic compartment receiving radon from not only arterial blood, but also from the small intestine and the compartment “other” which contains hepatic portal vein. Fat is divided into two compartments, to represent short retention (fat 2) and long retention (fat 1) of radon. The uptake and retention in breast are described by glandular breast tissue ($breast_g$) and adipose breast tissue ($breast_a$) that are derived from studies on females and extrapolated to males.

The principal excretion path is through exhalation with other excretion pathways, e.g. urine and skin, being comparatively small. According to experimental studies, the rate of transfer from RT-air to environment is dependent on breathing rate but is for dosimetric purposes assumed to be constant. The radon concentration in RT-air is assumed to instantaneously reach equilibrium with environment radon concentration. The transfer rate of activity from environment to RT-air is given by $\lambda \cdot C_{enviroment} \cdot V_{RT\text{-}air}$ [$Bq \cdot d^{-1}$], where λ is the transfer rate from RT-air to environment, $C_{enviroment}$ is radon activity concentration in air and $V_{RT\text{-}air}$ is the age-dependent average volume of RT-air.

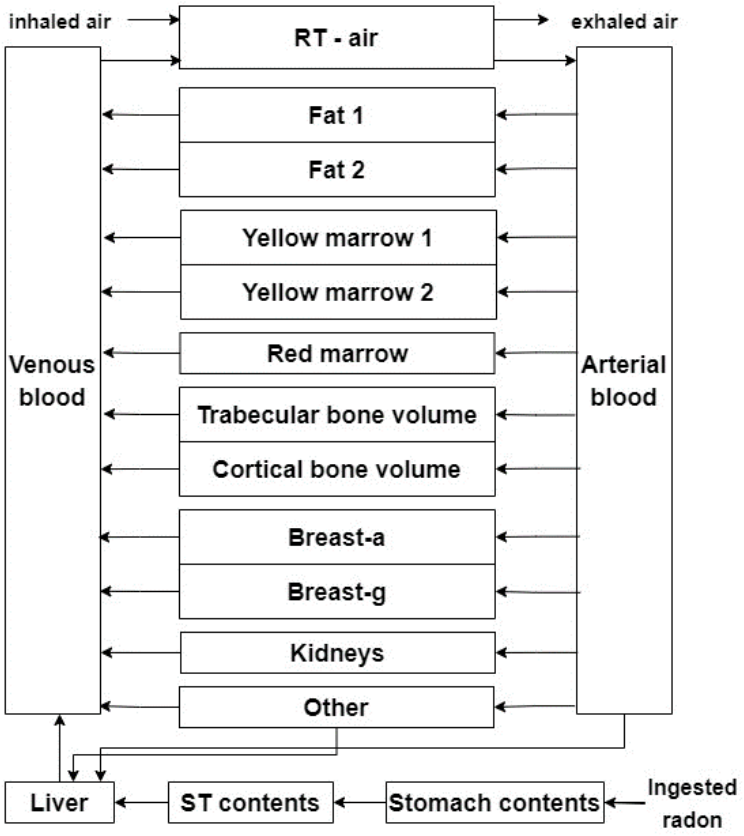

Figure 8. Structure of biokinetic model for radon. Redrawn from (Samuels et al., 2023).

B-2: Polonium

The structure for the systemic model for polonium is depicted in Figure 9 with associated age-independent transfer coefficients in Table 16.

The inhaled activity is assumed to enter blood in plasma 2, which has an outward transfer coefficient of 1000 d^{-1}, distributed by 80% and 20% to plasma 1 and kidneys 1 respectively. The absorption and reabsorption of material for the rest of the body occurs via plasma 1, which has a total transfer coefficient of 100 d^{-1}. 6% of the element in plasma 1 is removed to red blood cells (RBC) and 4% is cleared to plasma 3 that contains protein-bound polonium. Liver is divided into two compartments to take account of short and long retention in the organ. 17.5% of polonium in plasma 1 is cleared via short retention in liver 1. The passage from plasma 1 to liver 1 and small intestine contents is assumed to be the only source of endogenous faecal excretion. 17.5% is cleared to liver 2. Also, the kidney is partitioned into two compartments, kidney 1 and kidney 2, that are assigned an inward transfer coefficient of 5% each. Kidney 1 represents the filtration of material in the glomerulus with further removal to urine bladder contents. Kidney 2 is used to take account of the reabsorption of material into plasma 1. The two compartments associated with skeleton, red marrow and bone surface receive 4% and 1.5% respectively of material leaving plasma 1. The gonads, comprising of testes and ovaries are described with one compartment, and have transfer coefficients 0.1 d^{-1} for testes and 0.05 d^{-1} for ovaries. The other tissues are summarized with

the compartment other, to which the associating transfer coefficient is assigned 32.35 d^{-1}. The reabsorption and particle transfer from a compartment in the systemic model is based on the removal half-time of the element from the compartment (ICRP, 2017).

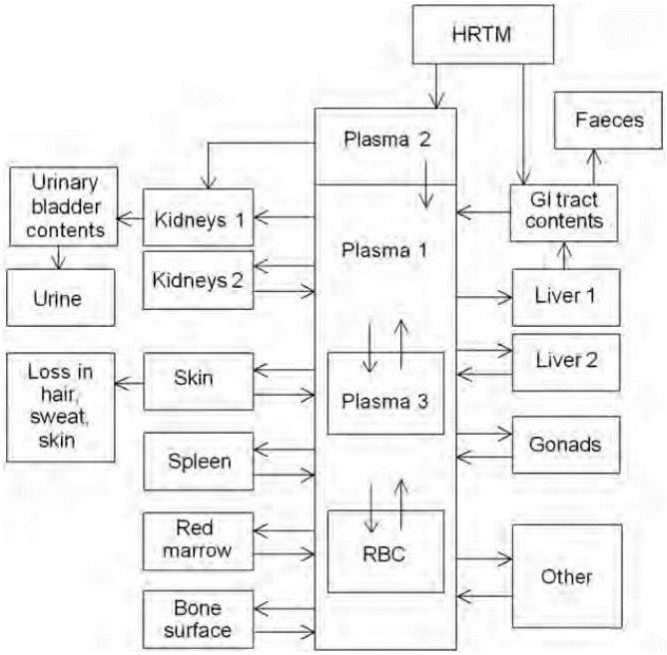

Figure 9. Systemic model for polonium. Taken from figure 11.1 of ICRP Publication 137 (2017). Used with permission from ICRP.

Table 16. Transfer coefficients between compartments in systemic model for polonium. Values for transfer coefficients are taken from table 11.3 in ICRP Publication 137 (2017). The transfer coefficients are same for workers and members of the public of all ages.

From	To	Transfer coefficient [d^{-1}]
Plasma 2	Plasma 1	800
Plasma 2	Kidney 1	200
Plasma 1	Plasma 3	4
Plasma 1	RBC	6
Plasma 1	Liver 1	17.5
Plasma 1	Liver 2	17.5
Plasma 1	Kidney 1	5
Plasma 1	Kidney 2	5
Plasma 1	Skin	5
Plasma 1	Red marrow	4
Plasma 1	Bone surface	1.5
Plasma 1	Spleen	2
Plasma 1	Testes	0.1
Plasma 1	Ovaries	0.05
Plasma 1	Other	32.35
Plasma 3	Plasma 1	0.0099

RBC	Plasma 1	0.099
Liver 1	Small intestine contents	0.139
Liver 2	Plasma 1	0.099
Kidney 1	Urinary bladder contents	0.173
Kidney 2	Plasma 1	0.099
Skin	Plasma 1	0.00693
Skin	Excreta	0.00693
Red marrow	Plasma 1	0.099
Bone surface	Plasma 1	0.0231
Spleen	Plasma 1	0.099
Testes	Plasma 1	0.0139
Ovaries	Plasma 1	0.0139
Other	Plasma 1	0.099

B-3: Bismuth

The structure of the systemic model for Bismuth is depicted in Figure 10, with corresponding age-independent transfer coefficients in Table 17. The rate of activity leaving the plasma is 400 d^{-1}. Three quarters are removed via the rapid extracellular fluid soft tissue (ST0). The remaining quarter is distributed between other tissues as followed: 20% to urinary bladder contents, 4% to right colon contents, 0.5% to RBC, 4.2% to intermediate turn-over soft tissue (ST1), 1.3% to slow turn-over soft tissue (ST2), 30% to liver 1, 30% to urinary path (kidneys), 5% to other kidney tissues and 2.5% to trabecular bone surface and cortical bone surface each (ICRP, 2017).

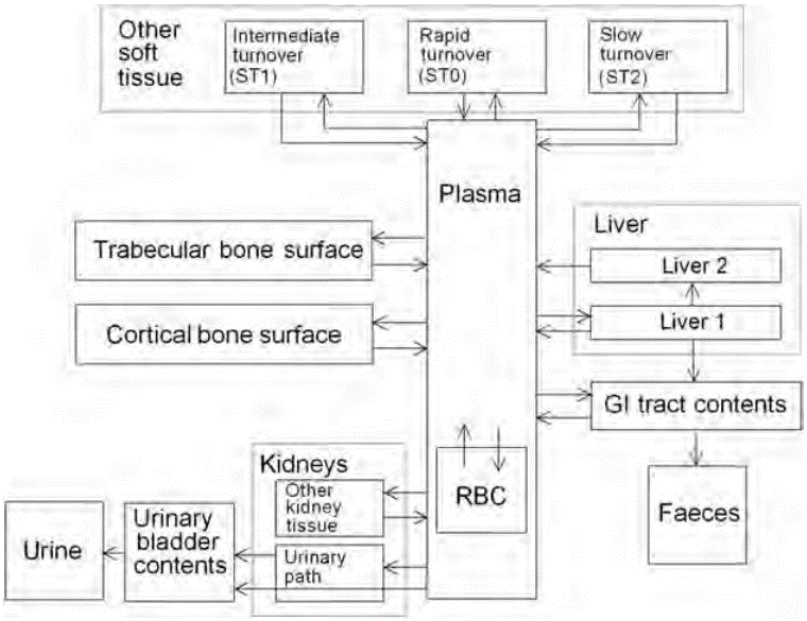

Figure 10. Systemic biokinetic model for Bismuth. Taken from Figure 10.1. in ICRP Publication 137 (2017). Used with permission from ICRP.

Table 17. Transfer coefficients for compartments in systemic model for Bismuth. Taken from Table 10.3 in ICRP Publication 137 (2017). The transfer coefficients are same for workers and members of the public of all ages.

From	To	Transfer coefficient [d^{-1}]
Plasma	Urinary bladder contents	20
Plasma	Right colon contents	4
Plasma	RBC	0.5
Plasma	ST0	300
Plasma	ST1	4.2
Plasma	ST2	1.3
Plasma	Liver 1	30
Plasma	Urinary path (kidneys)	30
Plasma	Other kidney tissue	30
Plasma	Cortical bone surface	2.5
Plasma	Trabecular bone surface	2.5
RBC	Plasma	0.173
ST0	Plasma	66.54
ST1	Plasma	0.0347
ST2	Plasma	0.00116
Liver 1	Small intestine contents	0.208
Liver 1	Liver 2	0.139
Liver 2	Plasma	0.0693
Urinary path (kidneys)	Urinary bladder contents	0.693
Other kidney tissue	Plasma	0.139
Cortical bone surface	Plasma	0.0347
Trabecular bone surface	Plasma	0.0347

B-4: Lead

Figure 11 shows the structure of systemic model for lead with transfer rates quoted in Table 18, given by ICRP Publication 137. The tabulated transfer rates are valid for the reference worker and adult member of the public (2017). Age-specific transfer rates for members of the public are in table A-4 of ICRP Publication 67 (1993a). The biokinetic model applied in ICRP publication 137 is a simplification of a model developed by Leggett (Leggett, 1993), where the latter provided more detail of the initial behaviour of lead in plasma and its distribution in RBC and soft tissue. The biokinetic model described in ICRP Publication 137 has been applied in this study.

The following percentages are true for the reference worker. The assigned total transfer rate from plasma to other is 70 d^{-1}. A substantial portion of lead in plasma, approximately 31.66% and 40%, is cleared to ST0 and RBC respectively.

The four pathways for removal of lead from the body are urinal and faecal excretion, sweat and loss in hair, nails and skin. About 6% of lead in plasma is assumed to be removed through urinary excretion pathways that consist of compartments urinary path, urinary bladder contents and urine. 1% of the plasmatic lead enters intestinal contents directly

through right colon contents. 45% of the deposition in the liver (Liver 1) is cleared to the small intestine. The remaining body excretion pathways, namely sweat and loss in hair, skin and nails comprises 0.6% and 0.4% of the plasmatic lead respectively.

Liver and kidney are each described with two compartments to take account of short and long retention in the organs. The short retention in liver is depicted with Liver 1, that receives 7% of the lead in the plasma. 10% of the deposited activity in liver is cleared to Liver 2, while the remaining 90% is distributed equally between small intestine and reabsorption into blood. The two compartments of kidney are urinary path (short retention) and other kidney tissues (long retention), that receive 3.5% and 0.035% of plasmatic lead respectively (ICRP, 2017).

To represent other soft tissues, the compartments ST0, ST1 and ST2 are used that stand for fast, intermediate and slow reabsorption of material to the blood respectively. These compartments include tissues such as fat, skin and skeletal muscle, but are based on the element's kinetics. Ergo they cannot be given precise anatomical definitions (Leggett, 1993). The clearance rate of material to ST0, ST1 and ST2 stand for 31.66%, 1% and 0.2% of the total outflow transfer coefficient from plasma.

The clearance rate to bone surface constitutes 12.5% of the total outflow from plasma, with approximately 6.9% transferred to trabecular bone surface and 5.6% transferred to cortical bone surface. The transfer rate from exchangeable cortical/trabecular volume is 1 d^{-1}, that is distributed equally between bone surface and nonexchangeable bone volume (ICRP, 2017).

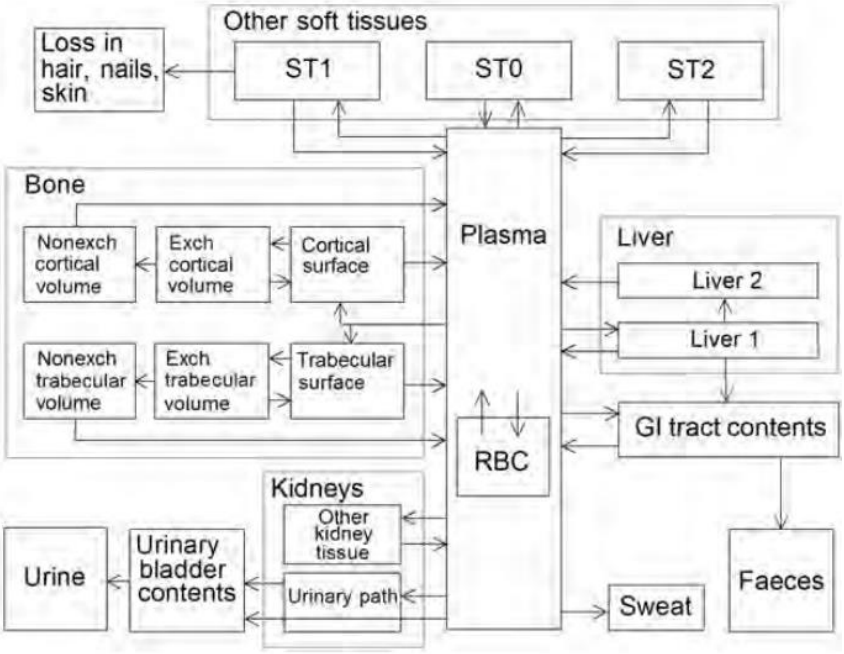

Figure 11. Structure over systemic biokinetic model for lead. Taken from figure 9.1. in ICRP Publication 137 (2017). Used with permission from ICRP.

Table 18. Transfer coefficients for compartments in the systemic model for lead. Taken from table 9.3. in ICRP Publication 137 (2017). The transfer coefficients for adult person and worker are same.

From	To	Transfer coefficients [d^{-1}]
Plasma	Urinary bladder contents	1.75
Plasma	Right colon contents	0.7
Plasma	Trabecular bone surface	4.86
Plasma	Cortical bone surface	3.89
Plasma	ST0	22.16
Plasma	ST1	0.7
Plasma	ST2	0.14
Plasma	Liver 1	4.9
Plasma	Urinary path	2.45
Plasma	Other kidney tissue	0.0245
Plasma	RBC	28
Plasma	Excreta (sweat)	0.42
RBC	Plasma	0.139
Trabecular bone surface	Plasma	0.5
Trabecular bone surface	Exch trabecular bone surface	0.5
Cortical bone surface	Plasma	0.5
Cortical bone surface	Exch cortical bone surface	0.5
Exch trabecular bone surface	Trabecular bone surface	0.0185
Exch trabecular bone surface	Nonexch trabecular bone surface	0.5
Exch cortical bone surface	Cortical bone surface	0.0185
Exch cortical bone surface	Exch cortical bone surface	0.0046
Nonexch bone surface	Plasma	0.000493
Nonexch cortical bone surface	Plasma	0.0000821
Liver 1	Plasma	0.0312
Liver 1	SI contents	0.0312
Liver 1	Liver 2	0.00693
Liver 2	Plasma	0.0019
Urinary path	Plasma	0.0019
Other kidney tissue	Urinary bladder contents	0.139
ST0	Plasma	0.0019
ST1	Plasma	7.39
ST2	Plasma	0.00038
ST1	Excreta (hair, skin, nails)	0.00277

B-5: Treatment of radionuclide as progeny of lead

Treatment of an arbitrary radionuclide as progeny of a preceding radon chain member is the same as if the radionuclide were a progeny of lead. Table 19 list the compartments and

associated transfer coefficients that need to be introduced in each element-specific systemic model to take account of the element as a progeny of lead. The supplementary compartments are often present in the preceding chain member's systemic models but absent in the model of the working element. For lead, the added compartments are thought to be part of the soft tissue compartments (ST0, ST1 and ST2). To compensate for the changes and ensure invariant total outflow from plasma, 2.5% is reduced from each soft tissue compartment. Similarly, the same is applied for bismuth, where the transfer rate from plasma to ST1 is reduced from 4.2 d^{-1} to 3.576 d^{-1}. The modified transfer rated from plasma to ST0, ST1 and ST2 are shown in Table 21. Other modifications include connecting the alimentary tract to plasma 2 instead of plasma 1 for polonium.

Table 19. Supplementary compartments with associated transfer coefficients for treatment of radionuclide as progeny of lead. For Pb the transfer coefficients from soft tissue (ST0, ST1 and ST2) correspond to the age-specific turnover rate. The values of transfer coefficients are collated based on associated text sections in ICRP Publication137 (2017) describing the changes that need to be introduced. NC = not changed; Ncbv = Nonexchangeable cortical bone volume; Ntbv = Nonexchangeable trabecular bone volume.

From	To	Transfer coefficient [d^{-1}]		
		Po	**Pb**	**Bi**
ST0	Plasma 2	0.099	Turnover rate	NC
ST1	Plasma 2	0.099	Turnover rate	NC
ST2	Plasma 2	0.099	Turnover rate	NC
Plasma	Red marrow		0.42	0.3
Plasma	Skin		0.14	0.3
Plasma	Spleen		0.021	0.02
Plasma	Testes		0.00035	0.003
Plasma	Ovaries		0.0014	0.001
Plasma	ST0		Table 21	NC
Plasma	ST1		Table 21	3.576
Plasma	ST2		Table 21	NC
Red marrow	Plasma		0.0019	0.0347
Skin	Plasma		0.0019	0.0347
Spleen	Plasma		0.0019	0.0347
Testes	Plasma		0.0019	0.0347
Ovaries	Plasma		0.0019	0.0347
Ncbv	Plasma			0.0000821
Ntbv	Plasma			0.000493

B-6: Treatment of radionuclide as progeny of radon

To take account of radioactive progeny of radon, four compartments need to be added to the modified systemic model of lead progeny. These compartments are explicit to the systemic model of radon and consist of fat 1, fat 2, adipose breast tissue ($breast_a$) and glandular breast tissue ($breast_g$). The supplementary compartments are assumed to be part of the compartment 'other' for polonium and ST1 for bismuth and lead. For an invariant total outflow from plasma, the sum of the transfer coefficients of the added compartments needs to be subtracted from the transfer coefficients of other and ST1. In addition, the radioactive progeny produced in compartments representing venous blood, arterial blood

and respiratory tract air are assumed to transfer to the central plasma and environment with a rate of 1000 d^{-1}. The values for the transfer rates are shown in Table 20. The modified transfer rates from plasma to ST1 are shown in Table 21.

Table 20. Supplementary compartments with associated transfer coefficients for treatment of radioactive progeny of radon. NC = not changed. For Pb the transfer coefficients from soft tissue (ST0, ST1 and ST2) correspond to the age-specific turnover rate. The values of transfer coefficients are collated based on associated text sections in ICRP Publication137 (2017) describing the changes that need to be introduced.

From	To	Transfer coefficient [d^{-1}]		
		Po	**Pb**	**Bi**
Plasma 1	Fat 1	2.1		
Plasma 1	Fat 2	0.52		
Plasma 1	$breast_a$	0.0075		
Plasma 1	$breast_g$	0.0025		
Fat 1	Plasma 1	0.099		
Fat 2	Palsma 1	0.099		
$breast_a$	Plasma 1	0.099		
$breast_g$	Plasma 1	0.099		
Plasma 1	Other	29.72		
Plasma	Fat 1		0.2	0.2
Plasma	Fat 2		0.05	0.05
Plasma	$breast_a$		0.0009	0.0009
Plasma	$breast_g$		0.0003	0.0003
Fat 1	Plasma		0.00416	0.0347
Fat 2	Plasma		0.00416	0.0347
$breast_a$	Plasma		0.00416	0.0347
$breast_g$	Plasma		0.00416	0.0347
Plasma	ST0		Table 21	NC
Plasma	ST1		Table 21	3.3248
Plasma	ST2		Table 21	NC

Table 21. Transfer coefficients [d^{-1}] from plasma to soft tissues categorized into ST0, ST1 and ST2 by ICRP Publication 67 (1993a). The transfer coefficients are valid for modified biokinetic models in order to take account of lead as progeny of radon and as progeny of lead.

	Plasma → ST0	
Age group	Lead as progeny of lead	Lead as progeny of radon
3 months old	15.434	
1 year old	19.140	
5 years old	19.754	
10 years old	17.774	
15 years old	15.561	
adult	21.606	
	Plasma → ST1	
Age group	Lead as progeny of lead	Lead as progeny of radon
3 months old	0.4875	0.4373
1 year old	0.6045	0.5543
5 years old	0.624	0.5738
10 years old	0.5616	0.5114

15 years old	0.4914	0.4412
adult	0.6825	0.6323

	Plasma → ST2	
Age group	Lead as progeny of lead	Lead as progeny of radon
3 months old	0.0975	
1 year old	0.1209	
5 years old	0.1248	
10 years old	0.1121	
15 years old	0.0975	
adult	0.1365	

Appendix C: Polynomials describing fractional deposition in the lung regions

Table 22. Derived polynomials for fractional deposition, y, for different lung regions and activity size (x) distribution modes for adult male. Input data are derived fractional deposition by Klumpp and Bertelli (Klumpp & Bertelli, 2017). The polynomials have been derived by curve fitting in Excel (Microsoft Corporation). The polynomial for deposition fraction corresponding to unattached mode has in the implemented biokinetic model been replaced with the values of the fractional deposition corresponding to 1 nm particle size.

Lung region	**Activity size distribution mode**		
	Cluster mode (0,6–10 nm)	Nucleation mode (5–500 nm)	Accumulation mode (10–10 000nm)
ET_1	$y = -0{,}0104x^5 - 0{,}3116x^4 - 3{,}6724x^3 - 21{,}351x^2 - 61{,}387x - 69{,}922$	$y = -0.0001x^5-0.0018x^4-0.0083x^3+0.0152x^2+0.1447x+0.221$	$y = -0.0001x^5-0.0018x^4-0.0083x^3+0.0152x^2+0.1447x+0.221$
ET_2	$y = -0{,}0057x^5 - 0{,}1691x^4 - 1{,}9935x^3 - 11{,}588x^2 - 33{,}306x - 37{,}921$	$y = -7E\text{-}05x^5 - 0{,}001x^4 - 0{,}0044x^3 + 0{,}0091x^2 + 0{,}0798x + 0{,}1202$	$y = -7E\text{-}05x^5 - 0{,}001x^4 - 0{,}0044x^3 + 0{,}0091x^2 + 0{,}0798x + 0{,}1202$
BB	$y = -0{,}0025x^5 - 0{,}0704x^4 - 0{,}7708x^3 - 4{,}1247x^2 - 10{,}837x - 11{,}208$	$y = -0{,}0025x^5 - 0{,}0704x^4 - 0{,}7708x^3 - 4{,}1247x^2 - 10{,}837x - 11{,}208$	$y = 1E\text{-}05x^6 + 7E\text{-}05x^5 - 0{,}0002x^4 - 0{,}0015x^3 + 0{,}0006x^2 + 0{,}0079x + 0{,}0132$
bb	$y = 0{,}0218x^5 + 0{,}6756x^4 + 8{,}2675x^3 + 49{,}944x^2 + 148{,}81x + 175{,}13$	$y = -7E\text{-}06x^6 - 2E\text{-}05x^5 + 0{,}0002x^4 - 0{,}0008x^3 + 0{,}0006x^2 - 0{,}0042x + 0{,}0212$	$y = -7E\text{-}06x^6 - 2E\text{-}05x^5 + 0{,}0002x^4 - 0{,}0008x^3 + 0{,}0006x^2 - 0{,}0042x + 0{,}0212$
ALV	$y = -0{,}0059x^5 - 0{,}2055x^4 - 2{,}7881x^3 - 18{,}493x^2 - 59{,}692x - 74{,}434$	$y = 0{,}0006x^6 + 0{,}0077x^5 + 0{,}0223x^4 - 0{,}0466x^3 - 0{,}2679x^2 - 0{,}3661x - 0{,}0187$	$y = -0{,}0001x^6 + 6E\text{-}05x^5 + 0{,}003x^4 - 0{,}0045x^3 - 0{,}0131x^2 - 0{,}0147x + 0{,}1203$

Table 23. Derived polynomials for fractional deposition, y, for different lung regions and activity size (x) distribution modes for adult female. Input data are derived depositional fraction by Klumpp and Bertelli (Klumpp & Bertelli, 2017). The polynomials have been derived by curve fitting in Excel. The polynomial for deposition fraction corresponding to unattached mode has in the implemented biokinetic model been replaced with the values of the fractional deposition corresponding to 1 nm particle size.

Lung region	**Activity size distribution mode**		
	Cluster mode (0,6–10 nm)	Nucleation mode (5–500 nm)	Accumulation mode (10–10 000)
ET_1	$y = -0{,}0103x^5 - 0{,}3067x^4 - 3{,}6125x^3 - 20{,}986x^2 - 60{,}289x - 68{,}617$	$y = -0{,}0001x^5 - 0{,}0017x^4 - 0{,}0084x^3 + 0{,}0141x^2 + 0{,}1449x + 0{,}2254$	$y = -0{,}0001x^5 - 0{,}0017x^4 - 0{,}0084x^3 + 0{,}0141x^2 + 0{,}1449x + 0{,}2254$
ET_2	$y = -0{,}0057x^5 - 0{,}1707x^4 - 2{,}0114x^3 - 11{,}686x^2 - 33{,}574x - 38{,}209$	$y = -7E\text{-}05x^5 - 0{,}001x^4 - 0{,}0045x^3 + 0{,}0086x^2 + 0{,}0802x + 0{,}1229$	$y = -7E\text{-}05x^5 - 0{,}001x^4 - 0{,}0045x^3 + 0{,}0086x^2 + 0{,}0802x + 0{,}1229$
BB	$y = -0{,}0023x^5 - 0{,}064x^4 - 0{,}6864x^3 - 3{,}5825x^2 - 9{,}1313x - 9{,}1033$	$y = -5E\text{-}05x^6 - 0{,}001x^5 - 0{,}0072x^4 - 0{,}0248x^3 - 0{,}0417x^2 - 0{,}0305x + 0{,}0006$	$y = 1E\text{-}05x^6 + 7E\text{-}05x^5 - 0{,}0002x^4 - 0{,}0015x^3 + 0{,}0005x^2 + 0{,}0075x + 0{,}0132$
bb	$y = 0{,}0233x^5 + 0{,}7179x^4 + 8{,}7409x^3 + 52{,}54x^2 + 155{,}79x + 182{,}49$	$y = -1E\text{-}05x^6 - 2E\text{-}05x^5 + 0{,}0003x^4 - 0{,}0007x^3 + 0{,}0005x^2 - 0{,}0052x + 0{,}023$	$y = -1E\text{-}05x^6 - 2E\text{-}05x^5 + 0{,}0003x^4 - 0{,}0007x^3 + 0{,}0005x^2 - 0{,}0052x + 0{,}023$
ALV	$y = -0{,}0072x^5 - 0{,}2427x^4 - 3{,}2055x^3 - 20{,}785x^2 - 65{,}851x - 80{,}946$	$y = 0{,}0006x^6 + 0{,}0081x^5 + 0{,}0258x^4 - 0{,}0323x^3 - 0{,}2395x^2 - 0{,}3401x - 0{,}0161$	$y = -0{,}0001x^6 + 5E\text{-}05x^5 + 0{,}0029x^4 - 0{,}0041x^3 - 0{,}0124x^2 - 0{,}0153x + 0{,}1138$

Table 24. Derived polynomials for fractional deposition, y, for different lung regions and activity size (x) distribution modes for 15-year-old male. Input data are derived depositional fraction by Klumpp and Bertelli (Klumpp & Bertelli, 2017). The polynomials have been derived by curve fitting in Excel. The polynomial for deposition fraction corresponding to unattached mode has in the implemented biokinetic model been replaced with the values of the fractional deposition corresponding to 1 nm particle size.

Lung region	**Activity size distribution mode**		
	Cluster mode (0,6–10 nm)	Nucleation mode (5–500 nm)	Accumulation mode (10–10 000)
ET_1	$y = -0{,}0097x^5 - 0{,}2903x^4 - 3{,}4195x^3 - 19{,}862x^2 - 57{,}049x - 64{,}911$	$y = -0{,}0001x^5 - 0{,}0017x^4 - 0{,}0077x^3 + 0{,}0146x^2 + 0{,}1357x + 0{,}2067$	$y = -0{,}0001x^5 - 0{,}0017x^4 - 0{,}0077x^3 + 0{,}0146x^2 + 0{,}1357x + 0{,}2067$
ET_2	$y = -0{,}0058x^5 - 0{,}1735x^4 - 2{,}0474x^3 - 11{,}916x^2 - 34{,}287x - 39{,}069$	$y = -9E\text{-}05x^5 - 0{,}0011x^4 - 0{,}0041x^3 + 0{,}0117x^2 + 0{,}0815x + 0{,}117$	$y = -9E\text{-}05x^5 - 0{,}0011x^4 - 0{,}0041x^3 + 0{,}0117x^2 + 0{,}0815x + 0{,}117$
BB	$y = -0{,}0023x^5 - 0{,}0627x^4 - 0{,}6785x^3 - 3{,}5799x^2 - 9{,}2421x - 9{,}3541$	$y = -5E\text{-}05x^5 - 0{,}0014x^4 - 0{,}0122x^3 - 0{,}0315x^2 - 0{,}0408x + 0{,}0082$	$y = 2E\text{-}05x^6 + 1E\text{-}04x^5 - 0{,}0004x^4 - 0{,}0023x^3 + 0{,}001x^2 + 0{,}0124x + 0{,}0175$

bb	$y = 0{,}0199x^5 + 0{,}6162x^4 + 7{,}5447x^3 + 45{,}596x^2 + 135{,}9x + 159{,}97$	$y = -5E\text{-}06x^4 - 0{,}0011x^3 + 0{,}0023x^2 - 0{,}0025x + 0{,}0199$	$y = -5E\text{-}06x^4 - 0{,}0011x^3 + 0{,}0023x^2 - 0{,}0025x + 0{,}0199$
ALV	$y = -0{,}0247x^4 - 0{,}6045x^3 - 5{,}4213x^2 - 20{,}946x - 28{,}979$	$y = 0{,}0005x^6 + 0{,}006x^5 + 0{,}0155x^4 - 0{,}0546x^3 - 0{,}26x^2 - 0{,}3433x - 0{,}0193$	$y = -0{,}0001x^6 + 6E\text{-}05x^5 + 0{,}0028x^4 - 0{,}0045x^3 - 0{,}0123x^2 - 0{,}0113x + 0{,}1113$

Table 25. Derived polynomials for fractional deposition, y, for different lung regions and activity size (x) distribution modes for 15-year-old female. Input data are derived depositional fraction by Klumpp and Bertelli (Klumpp & Bertelli, 2017). The polynomials have been derived by curve fitting in Excel. The polynomial for deposition fraction corresponding to unattached mode has in the implemented biokinetic model been replaced with the values of the fractional deposition corresponding to 1 nm particle size.

Lung region	**Activity size distribution mode**		
	Cluster mode (0,6–10 nm)	Nucleation mode (5–500 nm)	Accumulation mode (10–10 000)
ET_1	$y = -0{,}0096x^5 - 0{,}2876x^4 - 3{,}3847x^3 - 19{,}644x^2 - 56{,}374x - 64{,}086$	$y = -0{,}0001x^5 - 0{,}0016x^4 - 0{,}0079x^3 + 0{,}0134x^2 + 0{,}1367x + 0{,}2132$	$y = -0{,}0001x^5 - 0{,}0016x^4 - 0{,}0079x^3 + 0{,}0134x^2 + 0{,}1367x + 0{,}2132$
ET_2	$y = -0{,}0061x^5 - 0{,}1832x^4 - 2{,}1636x^3 - 12{,}607x^2 - 36{,}325x - 41{,}46$	$y = -8E\text{-}05x^5 - 0{,}0011x^4 - 0{,}0042x^3 + 0{,}011x^2 + 0{,}082x + 0{,}1205$	$y = -8E\text{-}05x^5 - 0{,}0011x^4 - 0{,}0042x^3 + 0{,}011x^2 + 0{,}082x + 0{,}1205$
BB	$y = -0{,}0024x^5 - 0{,}0664x^4 - 0{,}7196x^3 - 3{,}8041x^2 - 9{,}8497x - 10{,}011$	$y = -5E\text{-}05x^5 - 0{,}0004x^4 - 0{,}0012x^3 + 0{,}0014x^2 + 0{,}0084x + 0{,}0147$	$y = 1E\text{-}05x^6 + 7E\text{-}05x^5 - 0{,}0002x^4 - 0{,}0019x^3 + 0{,}0004x^2 + 0{,}0112x + 0{,}0176$
bb	$y = 0{,}0199x^5 + 0{,}6148x^4 + 7{,}5175x^3 + 45{,}372x^2 + 135{,}05x + 158{,}77$	$y = 3E\text{-}05x^5 + 0{,}0002x^4 - 0{,}0015x^3 + 0{,}0005x^2 - 0{,}0021x + 0{,}022$	$y = 3E\text{-}05x^5 + 0{,}0002x^4 - 0{,}0015x^3 + 0{,}0005x^2 - 0{,}0021x + 0{,}022$
ALV	$y = -0{,}0241x^4 - 0{,}5878x^3 - 5{,}2636x^2 - 20{,}294x - 27{,}991$	$y = -0{,}0026x^5 - 0{,}0449x^4 - 0{,}2647x^3 - 0{,}6348x^2 - 0{,}6626x - 0{,}1184$	$y = -0{,}0001x^6 + 5E\text{-}05x^5 + 0{,}0028x^4 - 0{,}0042x^3 - 0{,}012x^2 - 0{,}0128x + 0{,}11$

Table 26. Derived polynomials for fractional deposition, y, for different lung regions and activity size (x) distribution modes for 10-year-olds. Input data are derived depositional fraction by Klumpp and Bertelli (Klumpp & Bertelli, 2017). The polynomials have been derived by curve fitting in Excel. The polynomial for deposition fraction corresponding to unattached mode has in the implemented biokinetic model been replaced with the values of the fractional deposition corresponding to 1 nm particle size.

Lung region	**Activity size distribution mode**		
	Cluster mode (0,6–10 nm)	Nucleation mode (5–500 nm)	Accumulation mode (10–10 000)
ET_1	$y = -0{,}0104x^5 - 0{,}3118x^4 - 3{,}6716x^3 - 21{,}325x^2 - 61{,}25x - 69{,}689$	$y = -5E\text{-}05x^5 - 0{,}0014x^4 - 0{,}0097x^3 + 0{,}0079x^2 + 0{,}1539x + 0{,}2634$	$y = -5E\text{-}05x^5 - 0{,}0014x^4 - 0{,}0097x^3 + 0{,}0079x^2 + 0{,}1539x + 0{,}2634$

ET_2	$y = -0{,}0057x^5 - 0{,}1708x^4 - 2{,}0126x^3 - 11{,}694x^2 - 33{,}603x - 38{,}254$	$y = -3E\text{-}05x^5 - 0{,}0008x^4 - 0{,}0052x^3 + 0{,}0044x^2 + 0{,}0831x + 0{,}1419$	$y = -3E\text{-}05x^5 - 0{,}0008x^4 - 0{,}0052x^3 + 0{,}0044x^2 + 0{,}0831x + 0{,}1419$
BB	$y = -0{,}0022x^5 - 0{,}0603x^4 - 0{,}6387x^3 - 3{,}2758x^2 - 8{,}1613x - 7{,}8959$	$y = -6E\text{-}05x^6 - 0{,}0011x^5 - 0{,}0076x^4 - 0{,}0266x^3 - 0{,}0456x^2 - 0{,}0349x - 0{,}0011$	$y = 1E\text{-}05x^6 + 5E\text{-}05x^5 - 0{,}0001x^4 - 0{,}0012x^3 - 1E\text{-}05x^2 + 0{,}0051x + 0{,}0118$
bb	$y = 0{,}0225x^5 + 0{,}6937x^4 + 8{,}4592x^3 + 50{,}921x^2 + 151{,}22x + 177{,}41$	$y = 2E\text{-}05x^4 - 0{,}0009x^3 + 0{,}0026x^2 - 0{,}0058x + 0{,}0169$	$y = 2E\text{-}05x^4 - 0{,}0009x^3 + 0{,}0026x^2 - 0{,}0058x + 0{,}0169$
ALV	$y = -0{,}0244x^4 - 0{,}5933x^3 - 5{,}2755x^2 - 20{,}184x - 27{,}601$	$y = -0{,}0003x^6 - 0{,}0106x^5 - 0{,}1208x^4 - 0{,}6227x^3 - 1{,}5293x^2 - 1{,}7865x - 0{,}67$	$y = -0{,}0011x^4 - 0{,}0043x^3 + 0{,}0196x^2 - 0{,}0152x + 0{,}0588$

Table 27. Derived polynomials for fractional deposition, y, for different lung regions and activity size (x) distribution modes for 5-year-olds. Input data are derived depositional fraction by Klumpp and Bertelli (Klumpp & Bertelli, 2017). The polynomials have been derived by curve fitting in Excel. The polynomial for deposition fraction corresponding to unattached mode has in the implemented biokinetic model been replaced with the values of the fractional deposition corresponding to 1 nm particle size.

Lung region	**Activity size distribution mode**		
	Cluster mode (0,6–10 nm)	Nucleation mode (5–500 nm)	Accumulation mode (10–10 000)
ET_1	$y = -0{,}0105x^5 - 0{,}3141x^4 - 3{,}692x^3 - 21{,}403x^2 - 61{,}368x - 69{,}725$	$y = -7E\text{-}05x^5 - 0{,}0015x^4 - 0{,}0096x^3 + 0{,}0097x^2 + 0{,}1548x + 0{,}2571$	$y = -7E\text{-}05x^5 - 0{,}0015x^4 - 0{,}0096x^3 + 0{,}0097x^2 + 0{,}1548x + 0{,}2571$
ET_2	$y = -0{,}0057x^5 - 0{,}1707x^4 - 2{,}0066x^3 - 11{,}63x^2 - 33{,}342x - 37{,}877$	$y = -4E\text{-}05x^5 - 0{,}0008x^4 - 0{,}0052x^3 + 0{,}0052x^2 + 0{,}0833x + 0{,}1385$	$y = -4E\text{-}05x^5 - 0{,}0008x^4 - 0{,}0052x^3 + 0{,}0052x^2 + 0{,}0833x + 0{,}1385$
BB	$y = -0{,}002x^5 - 0{,}0525x^4 - 0{,}5099x^3 - 2{,}3148x^2 - 4{,}8067x - 3{,}4334$	$y = -0{,}0001x^6 - 0{,}0023x^5 - 0{,}016x^4 - 0{,}0556x^3 - 0{,}0973x^2 - 0{,}0805x - 0{,}0157$	$y = -7E\text{-}06x^5 - 1E\text{-}05x^4 - 0{,}0004x^3 + 2E\text{-}06x^2 + 0{,}0023x + 0{,}0107$
bb	$y = 0{,}0284x^5 + 0{,}8629x^4 + 10{,}374x^3 + 61{,}582x^2 + 180{,}43x + 208{,}97$	$y = -2E\text{-}05x^6 - 7E\text{-}05x^5 + 0{,}0004x^4 + 4E\text{-}05x^3 + 0{,}0006x^2 - 0{,}0096x + 0{,}0206$	$y = -2E\text{-}05x^6 - 7E\text{-}05x^5 + 0{,}0004x^4 + 4E\text{-}05x^3 + 0{,}0006x^2 - 0{,}0096x + 0{,}0206$
ALV	$y = -0{,}0116x^5 - 0{,}3696x^4 - 4{,}6469x^3 - 28{,}822x^2 - 87{,}844x - 104{,}66$	$y = -0{,}0039x^5 - 0{,}0624x^4 - 0{,}3463x^3 - 0{,}8082x^2 - 0{,}8326x - 0{,}1748$	$y = -0{,}0001x^6 + 7E\text{-}06x^5 + 0{,}0028x^4 - 0{,}0028x^3 - 0{,}0104x^2 - 0{,}0224x + 0{,}1035$

Table 28. Derived polynomials for fractional deposition, y, for different lung regions and activity size (x) distribution modes for 1-year-olds. Input data are derived depositional fraction by Klumpp and Bertelli (Klumpp & Bertelli, 2017). The polynomials have been derived by curve fitting in Excel. The polynomial for deposition fraction corresponding to unattached mode has in the implemented biokinetic model been replaced with the values of the fractional deposition corresponding to 1 nm particle size.

Lung region	**Activity size distribution mode**		
	Cluster mode (0,6–10 nm)	Nucleation mode (5–500 nm)	Accumulation mode (10–10 000)
ET_1	$y = -0{,}0108x^5 - 0{,}3202x^4 - 3{,}763x^3 - 21{,}816x^2 - 62{,}569x - 71{,}127$	$y = 0{,}0001x^6 + 0{,}0008x^5 - 0{,}0016x^4 - 0{,}0204x^3 - 0{,}0027x^2 + 0{,}1842x + 0{,}3136$	$y = 0{,}0001x^6 + 0{,}0008x^5 - 0{,}0016x^4 - 0{,}0204x^3 - 0{,}0027x^2 + 0{,}1842x + 0{,}3136$
ET_2	$y = -0{,}0057x^5 - 0{,}1701x^4 - 1{,}9984x^3 - 11{,}583x^2 - 33{,}21x - 37{,}741$	$y = 6E\text{-}05x^6 + 0{,}0004x^5 - 0{,}0009x^4 - 0{,}011x^3 - 0{,}0014x^2 + 0{,}0992x + 0{,}1689$	$y = 6E\text{-}05x^6 + 0{,}0004x^5 - 0{,}0009x^4 - 0{,}011x^3 - 0{,}0014x^2 + 0{,}0992x + 0{,}1689$
BB	$y = 0{,}0131x^4 + 0{,}3201x^3 + 2{,}8724x^2 + 11{,}165x + 15{,}954$	$y = -0{,}0002x^6 - 0{,}0038x^5 - 0{,}0262x^4 - 0{,}089x^3 - 0{,}1542x^2 - 0{,}1281x - 0{,}0289$	$y = 1E\text{-}05x^6 + 3E\text{-}05x^5 - 0{,}0001x^4 - 0{,}0008x^3 + 0{,}0003x^2 + 0{,}0014x + 0{,}0105$
bb	$y = 0{,}0298x^5 + 0{,}8965x^4 + 10{,}664x^3 + 62{,}612x^2 + 181{,}38x + 207{,}69$	$y = -3E\text{-}05x^6 - 0{,}0001x^5 + 0{,}0006x^4 + 0{,}001x^3 + 0{,}0003x^2 - 0{,}014x + 0{,}0197$	$y = -3E\text{-}05x^6 - 0{,}0001x^5 + 0{,}0006x^4 + 0{,}001x^3 + 0{,}0003x^2 - 0{,}014x + 0{,}0197$
ALV	$y = -0{,}0124x^5 - 0{,}3868x^4 - 4{,}7785x^3 - 29{,}114x^2 - 87{,}16x - 102$	$y = -0{,}0058x^5 - 0{,}0875x^4 - 0{,}4641x^3 - 1{,}0565x^2 - 1{,}0834x - 0{,}2463$	$y = -0{,}0001x^6 - 5E\text{-}05x^5 + 0{,}0026x^4 - 0{,}0012x^3 - 0{,}0053x^2 - 0{,}0417x + 0{,}1024$

Table 29. Derived polynomials for fractional deposition, y, for different lung regions and activity size (x) distribution modes for 3 months old. Input data are derived depositional fraction by Klumpp and Bertelli (Klumpp & Bertelli, 2017). The polynomials have been derived by curve fitting in Excel. The polynomial for deposition fraction corresponding to unattached mode has in the implemented biokinetic model been replaced with the values of the fractional deposition corresponding to 1 nm particle size.

Lung region	**Activity size distribution mode**		
	Cluster mode (0,6–10 nm)	Nucleation mode (5–500 nm)	Accumulation mode (10–10 000)
ET_1	$y = -0{,}0107x^5 - 0{,}3174x^4 - 3{,}7205x^3 - 21{,}513x^2 - 61{,}546x - 69{,}797$	$y = 0{,}0001x^6 + 0{,}0008x^5 - 0{,}0016x^4 - 0{,}0205x^3 - 0{,}0026x^2 + 0{,}1848x + 0{,}3136$	$y = 0{,}0001x^6 + 0{,}0008x^5 - 0{,}0016x^4 - 0{,}0205x^3 - 0{,}0026x^2 + 0{,}1848x + 0{,}3136$
ET_2	$y = -0{,}0057x^5 - 0{,}1687x^4 - 1{,}9763x^3 - 11{,}421x^2 - 32{,}653x - 37{,}005$	$y = -0{,}0006x^4 - 0{,}0058x^3 - 7E\text{-}05x^2 + 0{,}0864x + 0{,}1662$	$y = -0{,}0006x^4 - 0{,}0058x^3 - 7E\text{-}05x^2 + 0{,}0864x + 0{,}1662$

BB	$y = 1{,}75E\text{-}02x^4 + 4{,}23E\text{-}01x^3 + 3{,}73E+00x^2 + 1{,}43E+01x + 2{,}01E+01$	$y = -0{,}0003x^6 - 0{,}0059x^5 - 0{,}0399x^4 - 0{,}1352x^3 - 0{,}2343x^2 - 0{,}1966x - 0{,}0488$	$y = -2E\text{-}05x^5 + 2E\text{-}05x^4 - 6E\text{-}05x^3 + 0{,}0003x^2 - 0{,}0016x + 0{,}0109$
bb	$y = 0{,}0251x^5 + 0{,}7415x^4 + 8{,}6273x^3 + 49{,}432x^2 + 139{,}46x + 155{,}33$	$y = -4E\text{-}05x^6 - 0{,}0002x^5 + 0{,}0008x^4 + 0{,}0014x^3 + 9E\text{-}06x^2 - 0{,}0176x + 0{,}0236$	$y = -4E\text{-}05x^6 - 0{,}0002x^5 + 0{,}0008x^4 + 0{,}0014x^3 + 9E\text{-}06x^2 - 0{,}0176x + 0{,}0236$
ALV	$y = -0{,}0104x^5 - 0{,}3193x^4 - 3{,}857x^3 - 22{,}953x^2 - 67{,}021x - 76{,}359$	$y = -0{,}0056x^5 - 0{,}0821x^4 - 0{,}4281x^3 - 0{,}9638x^2 - 0{,}9817x - 0{,}2249$	$y = -0{,}0001x^6 - 0{,}0001x^5 + 0{,}0019x^4 - 0{,}0003x^3 - 0{,}0021x^2 - 0{,}0389x + 0{,}0879$

References

Andersson, M., Johansson, L., Eckerman, K., & Mattsson, S. (2017). IDAC-Dose 2.1, an internal dosimetry program for diagnostic nuclear medicine based on the ICRP adult reference voxel phantoms. *EJNMMI Research*, *7*(1), 88. https://doi.org/10.1186/s13550-017-0339-3

Andersson, M., Leggett, R. W., Eckerman, K., Almén, A., & Mattsson, S. (2022). IDAC-Bio, A Software for Internal Dosimetry Based on the New ICRP Biokinetic Models and Specific Absorbed Fractions. *Health Physics*, *123*(2), 165-172. https://doi.org/10.1097/hp.0000000000001571

Baias, P. F., Hofmann, W., Winkler-Heil, R., Cosma, C., & Duliu, O. G. (2009). Lung dosimetry for inhaled radon progeny in smokers. *Radiation Protection Dosimetry*, *138*(2), 111-118. https://doi.org/10.1093/rpd/ncp183

Barrett, P. H. R., Bell, B. M., Cobelli, C., Golde, H., Schumitzky, A., Vicini, P., & Foster, D. M. (1998). SAAM II: Simulation, analysis, and modeling software for tracer and pharmacokinetic studies. *Metabolism - Clinical and Experimental*, *47*(4), 484-492. https://doi.org/10.1016/S0026-0495(98)90064-6

Bengtson, I. (2018). *ESTIMATION OF RADIATION EXPOSURE FROM NATURALLY OCCURRING RADIONUCLIDES IN FOOD AND FOODSTUFF.* [Master thesis, University of Gothenburg]. Gothenburg University Publications Electronic Archive. http://hdl.handle.net/2077/70340

BOICE JR, J. D. (2006). Ionizing Radiation In D. Schottenfeld & J. F. Fraumeni Jr. (Eds.), *Cancer epidemiology and prevention* (Third ed., pp. 275-276). Oxford University Press, Inc.

Brudecki, K., Li, W. B., Meisenberg, O., Tschiersch, J., Hoeschen, C., & Oeh, U. (2014). Age-dependent inhalation doses to members of the public from indoor short-lived radon progeny. *Radiation and Environmental Biophysics*, *53*(3), 535-549. https://doi.org/10.1007/s00411-014-0543-8

Darby, S., Hill, D., Auvinen, A., Barros-Dios, J. M., Baysson, H., Bochicchio, F., Deo, H., Falk, R., Forastiere, F., Hakama, M., Heid, I., Kreienbrock, L., Kreuzer, M., Lagarde, F., Mäkeläinen, I., Muirhead, C., Oberaigner, W., Pershagen, G., Ruano-Ravina, A., . . . Doll, R. (2005). Radon in homes and risk of lung cancer: collaborative analysis of individual data from 13 European case-control studies. *BMJ*, *330*(7485), 223. https://doi.org/10.1136/bmj.38308.477650.63

Darby, S., Hill, D., Deo, H., Auvinen, A., Barros-Dios, J. M., Baysson, H., Bochicchio, F., Falk, R., Farchi, S., Figueiras, A., Hakama, M., Heid, I., Hunter, N., Kreienbrock, L., Kreuzer, M., Lagarde, F., Mäkeläinen, I., Muirhead, C., Oberaigner, W., . . . Doll, R. (2006). Residential Radon and Lung cancer-detailed Results of a Collaborative Analysis of Individual Data on 7148 Persons with LUNG Cancer and 14 208 Persons without Lung Cancer from 13 Epidemiologic Studies in Europe. *Scandinavian Journal of Work, Environment & Health*, *32*(1), 1-84.

Ecolego. (2023, 2023-03-02). *Ecolego Wiki*. Retrieved 2023-10-03 from https://resources.facilia.se/ecolegowiki/doku.php

Harrison, J. (2009). Biokinetic and dosimetric modelling in the estimation of radiation risks from internal emitters. *Journal of Radiological Protection*, *29*(2A), A81. https://doi.org/10.1088/0952-4746/29/2A/S06

Harrison, J. D., & Marsh, J. W. (2020). ICRP recommendations on radon. *Annals of the ICRP*, *49*(1_suppl), 68-76. https://doi.org/10.1177/0146645320931974

Hofmann, W., Arvela, H., Harley, N., Marsh, J., McLaughlin, J., Röttger, A., & Tokonami, S. (2012). 3. Radon and Radon Progeny Inhalation and Resultant Doses. *Journal of the ICRU*, *12*(2), 29-53.

ICRP. (1993a). *Age-dependent doses to members of the public from intake of radionuclides: Part 2. Ingestion dose coefficients. ICRP Publication 67. Ann. ICRP 23* (3-4).

ICRP. (1993b). *Protection against radon-222 at home and at work. ICRP Publication 65. Ann. ICRP 23* (2).

ICRP. (1994). *Human Respiratory Tract Model for Radiological Protection. ICRP Publication 66. Ann. ICRP 24* (1-3).

ICRP. (1995). *Age-dependent Doses to Members of the Public from intake of Radionuclides - Part 4 Inhalation Dose Coefficients. ICRP Publication 71. Ann. ICRP 25* (3-4).

ICRP. (2006). *Human Alimentary Tract Model for Radiological Protection. ICRP Publication 100. Ann. ICRP 36* (1-2).

ICRP. (2007). *The 2007 Recommendations of the International Commission on Radiological Protection. ICRP Publication 103. Ann. ICRP 37* (2-4).

ICRP. (2008). *Nuclear Decay Data for Dosimetric Calculations. ICRP Publication 107. Ann. ICRP 38* (3).

ICRP. (2010). *Lung Cancer Risk from Radon and Progeny and Statement on Radon. ICRP Publication 115, Ann. ICRP 40* (1).

ICRP. (2014). *Radiological protection against radon exposure. ICRP Publication 126. Ann. ICRP 43* (3).

ICRP. (2015). *Occupational Intakes of Radionuclides: Part 1. ICRP Publication 130. Ann. ICRP 44* (2).

ICRP. (2016). *The ICRP computational framework for internal dose assessment for reference adults: specific absorbed fractions. ICRP Publication 133. Ann. ICRP 45* (2).

ICRP. (2017). *Occupational intakes of radionuclides: Part 3. ICRP Publication 137. Ann. ICRP 46* (3/4).

ICRP. (2020). *Paediatric Computational Reference Phantoms. ICRP Publication 143. Ann. ICRP 49* (1).

Isaksson, M. (2003). *Biokinetisk analys och modeller.* [Lecture notes]. Medical radiation sciences of University of Gothenburg.

Isaksson, M. (2017). *Environmental radioactivity and emergency preparedness*. Boca Raton, FL : CRC Press, Taylor & Francis Group.

James, A. C., Birchall, A., & Akabani, G. (2004). Comparative dosimetry of BEIR VI revisited. *Radiation Protection Dosimetry*, *108*(1), 3-26. https://doi.org/10.1093/rpd/nch007

Kendall, G. M., & Smith, T. J. (2002). Doses to organs and tissues from radon and its decay products. *Journal of Radiological Protection*, *22*(4), 389-406. https://doi.org/10.1088/0952-4746/22/4/304

Kendall, G. M., & Smith, T. J. (2005). Doses from radon and its decay products to children. *Journal of Radiological Protection*, *25*(3), 241. https://doi.org/10.1088/0952-4746/25/3/002

Klumpp, J., & Bertelli, L. (2017). KDEP: A Resource for Calculating Particle Deposition in the Respiratory Tract. *Health physics (1958)*, *113*(2), 110-121. https://doi.org/10.1097/HP.0000000000000679

Leggett, R., Marsh, J., Gregoratto, D., & Blanchardon, E. (2013). A generic biokinetic model for noble gases with application to radon. *Journal of Radiological Protection*, *33*(2), 413. https://doi.org/10.1088/0952-4746/33/2/413

Leggett, R. W. (1993). An Age-Specific Kinetic Model of Lead Metabolism in Humans. *Environmental Health Perspectives*, *101*(7), 598-616. https://doi.org/10.2307/3431645

Mohamed, A. (2004). Influence of radioactive aerosol and biological parameters of inhaled radon progeny on human lung dose. *Radiation Protection Dosimetry*, *113*(1), 115-122. https://doi.org/10.1093/rpd/nch429

NIST. *NIST Physical Measurement Laboratory. NIST Standard Reference Database 124* https://doi.org/ https://dx.doi.org/10.18434/T4NC7P

Porstendörfer, J. (1994). Properties and behaviour of radon and thoron and their decay products in the air. *Journal of Aerosol Science*, *25*(2), 219-263. https://doi.org/https://doi.org/10.1016/0021-8502(94)90077-9

Porstendörfer, J. (2001). Physical Parameters and Dose Factors of the Radon and Thoron Decay Products. *Radiation Protection Dosimetry*, *94*(4), 365-373. https://doi.org/10.1093/oxfordjournals.rpd.a006512

Rönnqvist, T. (2021). Radonova Laboratories AB, Uppsala. 2021:28 Analysis of Radon Levels in Swedish Dwellings and Workplaces.

Samuels, C., Marsh, J., & Leggett, R. (2023). An age- and sex-specific biokinetic model for radon*. *Journal of Radiological Protection*, *43*(4), 041502. https://doi.org/10.1088/1361-6498/acfb19

Sharma, S., Kumar, A., & Mehra, R. (2018). AGE-DEPENDENT INHALATION DOSE DUE TO EXPOSURE OF SHORT LIVED PROGENY OF RADON AND THORON FOR DIFFERENT AGE GROUPS IN JAMMU & KASHMIR, HIMALAYAS. *Radiation Protection Dosimetry*, *182*(4), 427-437. https://doi.org/10.1093/rpd/ncy084

SSM. (2023). Swedish Radiation Safety Authority. Referensnivå och gränsvärden för radon. Retrieved 2023-09-30, from https://www.stralsakerhetsmyndigheten.se/omraden/radon/referensniva-och-gransvarden-for-radon/

UKHSA. (2020). UK Health Security Agency. Taurus - The New Internal Dosimetry Software. Retrieved 2023-12-15, from https://www.ukhsa-protectionservices.org.uk/idcs/taurus/

UKHSA. (n.d.). UK Health Security Agency. Taurus. Retrieved 2023-12-15, from https://www.ukhsa-protectionservices.org.uk/cms/assets/gfx/content/resource_4976cs4fe5149039.pdf

UNSCEAR. (2000). UNSCEAR 2000 Report Volume I. Sources and effects of ionizing radiation. Report to the General Assembly with Scientific Annexes. *United Scientific Committee*

on the Effects of Atomic Radiation, *Annex B: Exposure from Natural Radiation Sources*, 107-108. https://www.unscear.org/unscear/en/publications/2000_1.html

UNSCEAR. (2009). UNSCEAR 2006 Report Volume II. Effects of ionizing radiation. *United Scientific Committee on the Effects of Atomic Radiation*, *Annex E: Sources-to-effects assessment for radon in homes and workplaces*, 203-210. https://www.unscear.org/unscear/en/publications/2006_2.html

WHO. (1986). Indoor Air Quality Research: Report on a WHO Meeting, Stockholm. 27–31. August 1984. World Health Organization, Copenhagen.

WHO. (2009). *WHO handbook on indoor radon: a public health perspective*. World Health Organization.

Winkler-Heil, R., Hofmann, W., Marsh, J., & Birchall, A. (2007). Comparison of radon lung dosimetry models for the estimation of dose uncertainties. *Radiation Protection Dosimetry*, *127*(1-4), 27-30. https://doi.org/10.1093/rpd/ncm339

Yu, K. N., Cheung, T. T. K., Haque, A. K. M. M., Nikezic, D., Lau, B. M. F., & Vucic, D. (2001). Radon progeny dose conversion coefficients for Chinese males and females. *Journal of Environmental Radioactivity*, *56*(3), 327-340. http://inis.iaea.org/search/search.aspx?orig_q=RN:33037168

Zhu, H., Li, J., Qiu, R., Pan, Y., Wu, Z., Li, C., & Zhang, H. (2018). Establishment of detailed respiratory tract model and Monte Carlo simulation of radon progeny caused dose. *Journal of Radiological Protection*, *38*(3), 990. https://doi.org/10.1088/1361-6498/aac987

Zock, C., Porstendörfer, J., & Reineking, A. (1996). The Influence of Biological and Aerosol Parameters of Inhaled Short-lived Radon Decay Products on Human Lung Dose. *Radiation Protection Dosimetry*, *63*(3), 197-206. https://doi.org/10.1093/oxfordjournals.rpd.a031530